May 2011

CELEBRATING 50 YEARS in 2010

DRAFT REPORT

CEMA Oil Sands Pit Lake Model

Submitted to:

Kyle Harrietha, Program Administrator
CEMA Reclamation Working Group
Suite 214, Morrison Building
9914 Morrison Street
Fort McMurray, AB T9H 4A4

Théo Charette, Technical Program Manager
CEMA Reclamation Working Group
18064 93 Avenue
Edmonton, AB, T5T 1Y1

REPORT

A world of capabilities delivered locally

Report Number: 09-1336-1008
Distribution:
Draft report delivered digitally

ERM

Golder Associates

Table of Contents

TABLES

FIGURES

APPENDICES

1.0 INTRODUCTION

This document describes the Oil Sands Pit Lake Model (OSPLM) that was developed for the Cumulative Environmental Management Association (CEMA). The model was developed specifically for predicting sediment and water quality in oil sands pit lakes. It can be used with pit lakes with or without Mature Fine Tailings (MFT). The OSPLM continues previous work commissioned by CEMA, with the addition of modules to incorporate sediment diagenesis, gas production and other related processes.

1.1 Background

The oil sands of Alberta, Canada contain approximately 170 billion barrels of proven oil reserves. In the Athabasca Oil Sands Region, north of Fort McMurray, the bitumen is close enough to the surface to be mined using conventional mining techniques. Presently, five mining projects are operating in the Athabasca Oil Sands Region, and other projects are at various stages of the regulatory application process.

Similar to mining operations in other resource industries (e.g., coal, metals and diamonds) oil sands mines will use pit lakes as part of their closure and reclamation strategy. Approximately 30 pit lakes will be created as part of approved and proposed oil sands mines in Alberta (Figure 1). In about half of these pit lakes, MFT will be placed in the pit before the pit is flooded with fresh water to create a lake. MFT is a mixture of fine clay materials that settle much more slowly than the coarser tailings (Mikula et al. 1996), and therefore pose challenges to reclamation. As MFT consolidates, water is released to the overlying water column, which must have a sufficient volume and residence time to assimilate and degrade these residual compounds.

Oil sands tailings contain residual organic compounds (Siddique et al. 2007), which must be contained or degraded prior to release of pit lake water to the surrounding environment. At present, all oil sands operations, with the exception of one upgrader, operate as closed-circuited systems. Oil sands pit lakes will be maintained within closed-circuited systems until they become certified by regulatory authorities as acceptable for release.

As part of the application for regulatory approval of an oil sands mine, pit lakes are assessed in the Environmental Impact Assessment (EIA), which predicts water quality in each pit lake and in receiving watercourses (e.g., Shell 2007). While these models incorporate the effects of water released from MFT using conservative assumptions regarding the quality of MFT release waters, there are currently no models available to (1) compute the relevant processes that occur within the MFT, (2) simulate the formation and release of gas bubbles and (3) simulate the interaction of gases within bubbles with constituents in the water column.

1.2 Previous Modelling

As a regional issue for oil sands operators, research on pit lake functioning has been conducted primarily by multi-stakeholder groups such as CEMA and the Canadian Oil Sands Network for Research and Development (CONRAD). Pit lake model development by CEMA mainly consisted of hydrodynamic modelling in Phase I (CEMA 2006) and hydrodynamic and water quality modelling in Phase II (CEMA 2007).

In Phase I, meromictic potential was examined using one-dimensional modelling in DYRESM (Antenucci and Imerito 2002) and RMA10 (King 1985). This modelling focussed on hydrodynamics, specifically the likelihood of meromixis under a variety of pit lake conditions and scenarios. Phase II continued the work on hydrodynamics, using CE-QUAL-W2 (Cole and Wells 2001) and RMA10 for two-dimensional modelling. Phase II modelling also examined potential water quality implications of MFT placement in pit lakes, although interactions within the MFT

were limited to prescribed consolidation and water release rates, with limited, externally-computed changes assumed to occur within the MFT.

1.3 Present Scope of Work

The present scope of work includes the development of a pit lake sediment diagenesis model. The model is designed specifically for oil sands pit lakes, although it could be applied to other systems. Its primary focus is to incorporate processes relevant to MFT as identified by CEMA's End Pit Lake Modelling Task Group (EPLMTG). These processes include chemical reactions within MFT that may result in the release of aqueous and gaseous compounds into the water column, leading to changes in pit lake water quality. The model simulates the anaerobic decay of these compounds and production of gases such as methane, which could alter the physiochemical nature of the pit lake water column. Processes included in the model are described more fully in Section 2.2.

Development of the OSPLM is a stepwise, research-based modelling exercise. During the present stage, the model framework and algorithms will be developed and made functional. Subsequently, model formulations will be validated, model limitations were analyzed and addressed, and the model will be refined to be used in full-scale operations. As such, it is recognized that the present stage of model development is "experimental", and future refinements of the model are anticipated. In addition, data obtained from future field and laboratory studies will be necessary for validation of the model framework and calibration of a working model. The present scope of work does not include model calibration or simulations, but Section 3 provides recommendations regarding follow-up studies that will assist in model setup and validation (note that validation in this context refers to validation of the model framework, not validation of simulated results).

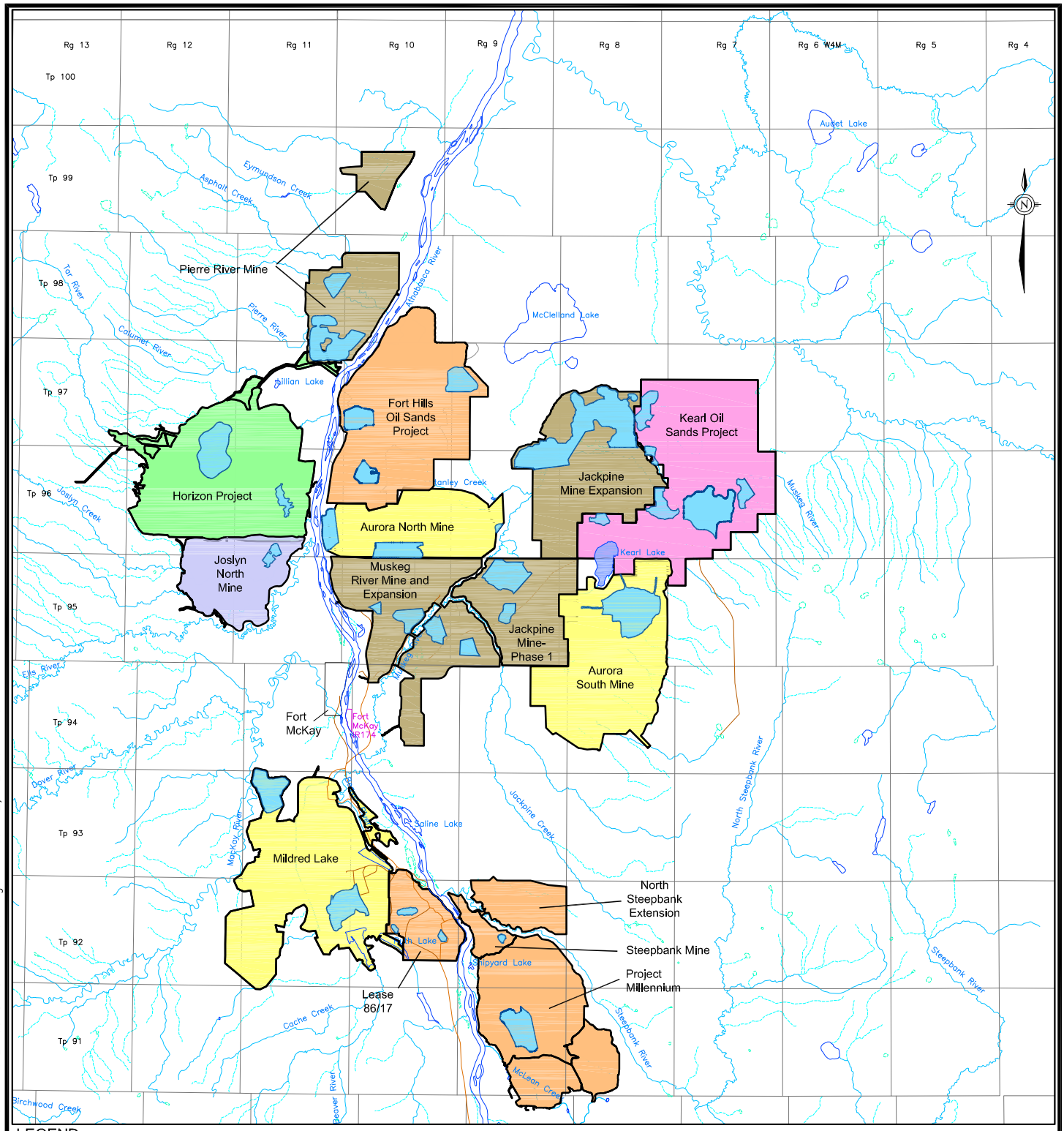

LEGEND

- ROADWAYS
- RIVERS AND STREAMS
- PIT LAKE

OIL SANDS OPERATORS

- CANADIAN NATURAL
- IMPERIAL OIL RESOURCES
- SHELL / ALBIAN SANDS
- SUNCOR ENERGY
- SYNCRUDE CANADA
- TOTAL E&P

DRAFT

NOTE: THESE ARE CONCEPTUAL DRAWINGS BASED ON INFORMATION FROM LONG-RANGE PLANS PROVIDED IN APPLICATIONS, EIAs AND OTHER UPDATE DOCUMENTS

REFERENCE

ALBERTA NTDB DIGITAL DATA OBTAINED FROM GEOMATICS CANADA, AUGUST 2001. DATUM: NAD 83
PROJECTION: UTM ZONE 12

10 0 10
SCALE 1:500,000 KILOMETRES

PROJECT

CEMA OIL SANDS PIT LAKE MODEL

TITLE

PLANNED PIT LAKES IN THE OIL SANDS REGION

Golder Associates
Calgary, Alberta

PROJECT	10.1336.1008.1000		FILE No.	101336100810000A001
DESIGN	JV	12/07/10	SCALE	AS SHOWN REV. 0
CADD	PSR	12/07/10		
CHECK	JV	12/07/10		
REVIEW				

FIGURE: 1

L:\2009\1336\09-1336-1008\Report A\Fig 1_Planned -Pit Lakes Oil Sands Area.dwg Jul 12, 2010 - 10:16am

2.0 OIL SANDS PIT LAKE MODEL

2.1 Model Platform

The freely-distributed CE-QUAL-W2 (W2) Version 3.6 (Cole and Wells 2008) forms the basis of the OSPLM. The default version of W2 is distributed by the Water Quality Research Group at Portland State University. This sediment diagenesis module was written in FORTRAN, and was added to the W2 code to create a single, fully-coupled model. The OSPLM includes upgrades such as ice-cover code modifications developed in the Phase II report (CEMA 2007). The OSPLM, including source code and executables, accompanies this report, and henceforth will be administered and distributed by CEMA.

2.2 Model Setup

The W2 code for version 3.6 was downloaded from the Portland Statue University website and setup on Intel Visual FORTRAN 11. Additional processes relevant to the OSPLM were programmatically added in different modules. These modules were written in separate FORTRAN files to keep the existing W2 code in its original form. This approach facilitates updates to new versions of W2 when they become available. The model setup is similar to the standard W2 approach: After reading the standard W2 variables, the model reads OSPLM-related variables (Figure 2), described in Appendix A. In addition to the standard W2 input files, OSPLM reads additional input files. Example input and output files are shown in Appendix B and C, respectively.

The sample application included with the report is set up for a 1 year simulation. A one-year simulation takes approximately 10 to 20 minutes to run, depending on the model resolution, computer speed and boundary conditions; high wind events can dramatically lower model timesteps.

2.3 Processes Included in the Model

At the scoping stage of this project, 14 processes were selected for inclusion in the OSPLM (Table 1 and Figure 3). These processes were identified as key drivers affecting pit lake water quality. In each subsection, identifiers P1 to P14 correspond to the processes listed in the second column of Table 1. Four of these processes, P4, P10, P11 and P12, are presently included in the standard version of W2, and are therefore not addressed in this report. The remaining processes are described below.

2.3.1 Tailings Consolidation, Lake Deepening and Porewater Release (P1, P2 & P3)

Tailings placed in the pit lakes will consolidate over time, releasing porewater into the overlying water column. The overall effect is that the pit lakes will deepen over time from their original bed elevations. The time for complete settling of MFT has been estimated at 125 to 150 years (Eckert et al. 1996), although methanogenesis may reduce this settling time considerably (Fedorak et al. 2003, Foght et al. 2010).

W2 is a traditional, fixed-grid model in which the bathymetric surface is static. In such a model, the initial bathymetric surface is used to create a grid on which hydrodynamic and transport computations are performed. The waterbody bathymetry and, consequently, the gridded representation of the bathymetric surface, are fixed throughout a simulation. To include the process of tailings consolidation and the resulting lake deepening, modifications to the W2 code were made to include a time-varying lake bottom. As modified, the model grid is developed from the initial lake bathymetry. During a simulation, the tailings consolidation is calculated based on user-defined rates that can vary spatially. Consolidation rates are not calculated by the OSPLM, but can be derived through a separate model, such as a finite strain or empirical model, then entered into the OSPLM. In each segment, a new bed elevation is calculated at each computational time step and compared to the initial bed

elevation. When the difference in the changed bed elevation and original bed elevation reaches a user-defined fraction of the bottom grid layer thickness, a new grid layer is added.

During consolidation, tailings bed porosity and total pore volume are calculated based on the consolidation rate. A volume of porewater, equal to the change in total pore volume since the previous timestep, is expressed from the tailings. This amount of porewater is released into the overlying water column along with porewater constituents. The porewater constituents may include the default chemicals, described in Section 2.3.2, as well as generic constituents and generic Biochemical Oxygen Demand (BOD) groups. Generic constituents and BOD groups that are defined in the sediment compartment will be transferred to the water column, where they will link in with the standard W2 variables. Generic constituents and BOD groups must be defined in both compartments for the model to recognize these constituents.

The process of consolidation, including layer addition and porewater release, continues throughout the simulation. Since the consolidation rate is user-defined, consolidation can be deactivated after a specified period by entering a rate of zero in the consolidation input file.

A conceptual diagram of tailings consolidation and its relationship to model grid additions is shown in Figure 4.

2.3.2 Tailings Gas Production (P4)

Prior to the early 1990s, methanogenesis had not been observed in oil sands tailings facilities. Although methanogens and sulfate-reducing bacteria had been observed in tailings samples, laboratory analyses suggested that methanogens were not likely to be active at ambient conditions in these facilities (Foght et al. 1985, Sobolewski 1992). In subsequent years, methanogenesis began to occur in the Mildred Lake Settling Basin (MLSB) at the Syncrude Canada Ltd. oil sands operation. The reason for the time lag and onset of methanogenesis is not known, but it may have been due to the depletion of sulfate, which allowed carbon to overtake sulfur as the dominant electron acceptor, or it may have been due to input of fresh tailings that contained naphtha compounds.

Since the onset of methanogenesis, the MLSB has produced significant amounts of gases, including methane. It has been estimated that 2% to 5% (v/v) of Mildred Lake was comprised of trapped and dissolved gases, and that gases contained 20% to 60% methane, which escaped MLSB at approximately 12 g CH_4/m^2 (Holowenko et al. 2000). Holowenko et al. (2000) also experimented with sulfate addition, and found that methanogens were outcompeted by sulfate reducing bacteria, and suggested that an anticipated shift to gypsum-amended tailings might result in higher concentrations of sulfate in the tailings and a concomitant decrease in methanogenesis. Sulfate inhibition of methane production was confirmed by subsequent work, in which methanogenesis was found to occur when sulfate was consumed to levels below 20 mg/L (Fedorak et al. 2002).

Studies have been conducted to determine the carbon source in methane-producing tailings, and these studies generally ruled out large organic molecules such as naphthenic acids. Holowenko et al. (2001) examined methanogenesis rates in the presence of various concentrations of naphthenic acids, and concluded that naphthenic acids were not likely the primary carbon source of methane in tailings ponds. Furthermore, naphthenic acids did not inhibit methanogenesis due to toxicity at concentrations likely to be found in tailings ponds. Holowenko (2000) amended tailings with bitumen and also observed no significant increase in methanogenesis, indicating that bitumen was not the primary source of carbon in methanogenesis. Haveroen et al. (2005) found that polyacrylamide may contribute to methanogenesis by providing a source of nitrogen, but the carbon was not utilized.

Figure 2: Flowchart showing OSPLM related code modifications to W2

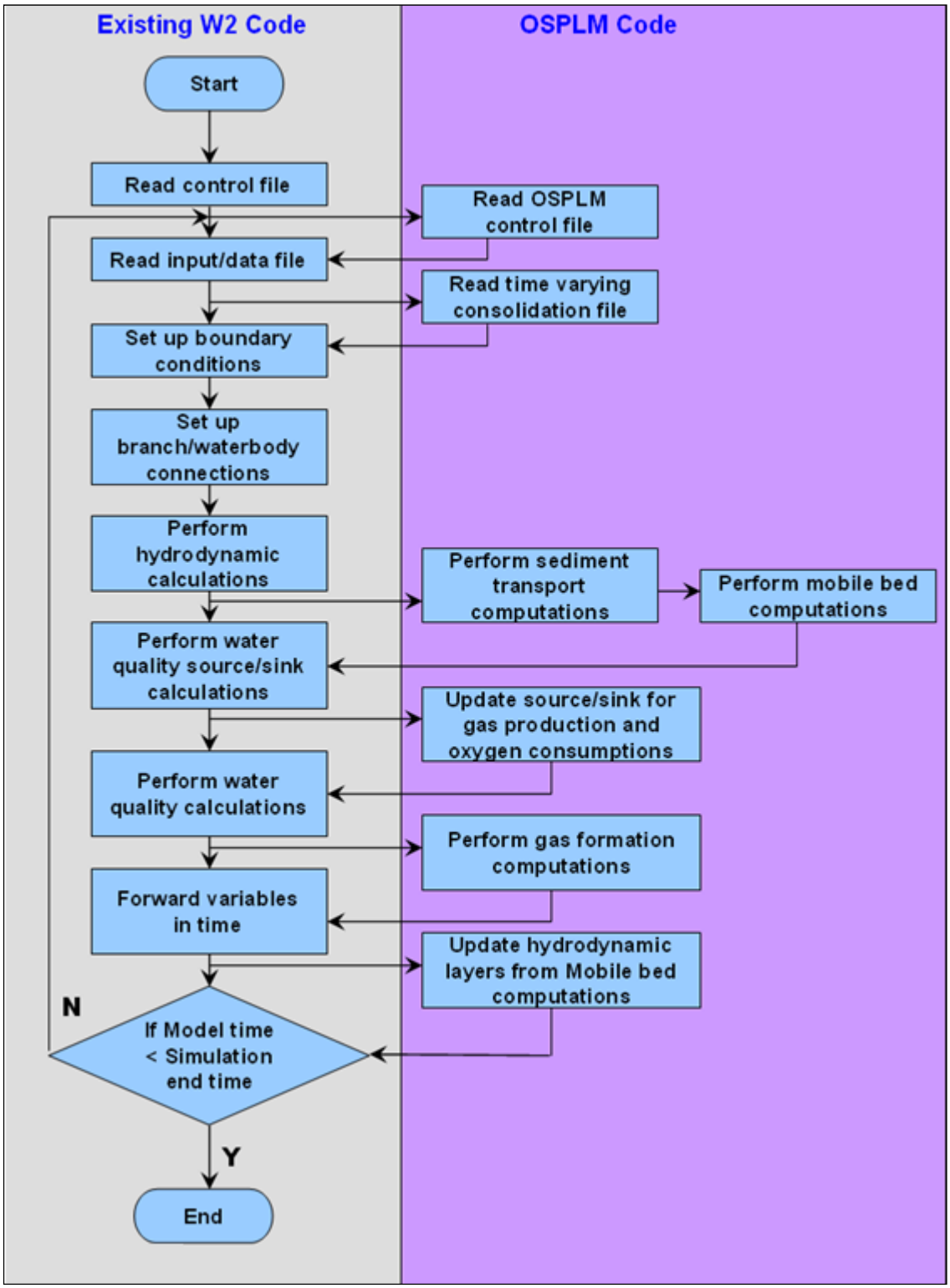

Table 1: Processes Included in the Oil Sands Pit Lake Model

Process	ID	Already in W2?	Approach
Tailings consolidation	P1	No	The mobile bed includes bed consolidation routines for the tailings consolidation. Tailings consolidation rates are provided to the W2 model using a time series input file. These rates are used to compute the evolving sediment bed. The same consolidation rate along with the mass and volume balance analysis are used to compute the porewater release and gas production.
Lake deepening	P2	No	As part of the sediment compartment representing the tailings, a dynamically-linked sediment bed model was added in W2 to model the mobile bed. The consolidation rates provide the time-varying elevation of the mobile bed which in turn are linked dynamically with the hydrodynamic model.
Porewater release	P3	No	Porewater release was added with the consolidation of tailings. Tailings consolidation rates are provided to the W2 model using a timeseries input file. These rates are used to compute the evolving sediment bed. The same consolidation rate along with the mass and volume balance analysis are used to compute the porewater release and gas production.
Tailings gas production	P4	No	Additional source/sink terms were added to compute the gas production from the tailings deposits by including a gas production module
Bubbling to surface	P5	No	Tailings gas release from the bed, its travel through the water column and its eventual release from the surface were added.
Unconsolidated sediment resuspension	P6	No	A sediment compartment with sediment resuspension was added. The sediment compartment performs bed elevation calculations based on mass balance (net deposition and resuspension) and tailings consolidation.
Erosion	P7	Yes	A simplified sediment resuspension algorithm is currently used in W2. The same resuspension algorithm is used for tailings resuspension in the OSPLM.
Water clarity (non-algal)	P8	No	A separate constituent representing water turbidity was added.
Oxygen consumption by released gases	P9	No	Additional source/sink terms were added to account for O_2 consumption. Gases released by tailings consolidation were modelled within the gas production module that interact with oxygen in the water column.
Chemical oxygen demand	P10	Yes	Process already available and functional in W2.
Biological oxygen demand	P11	Yes	Process already available and functional in W2. Generic BOD substances were added to sediment that exert BOD in water column when released from sediment.
Variable lake-bottom oxygen consumption	P12	Yes	Sediment oxygen demand is already available in W2; modifications were added to account for tailings-related demand.
Fluid fine tails layer	P13	No	A dense layer of inorganic suspended solids was added above the sediment bed. The model code was modified to allow solids to drop as new layers are added. A switch was added to deactivate the FFT layer.
Salt rejection	P14	No	Salt rejection was added to OSPLM.

Figure 3: Conceptual Diagram of Processes Included in the Oil Sands Pit Lake Model

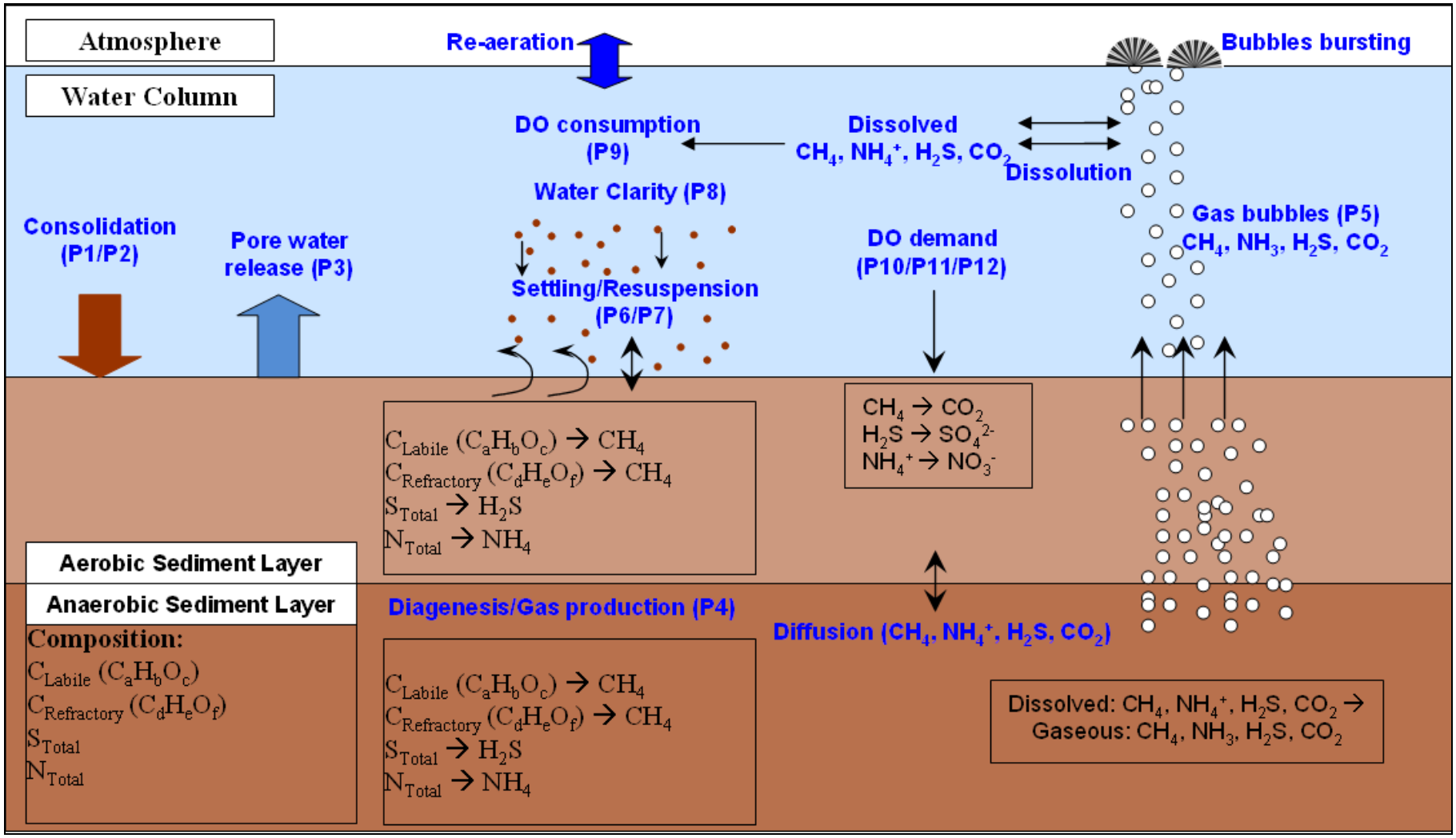

Figure 4: Conceptual Diagram of Tailings Consolidation and Grid Layer Change

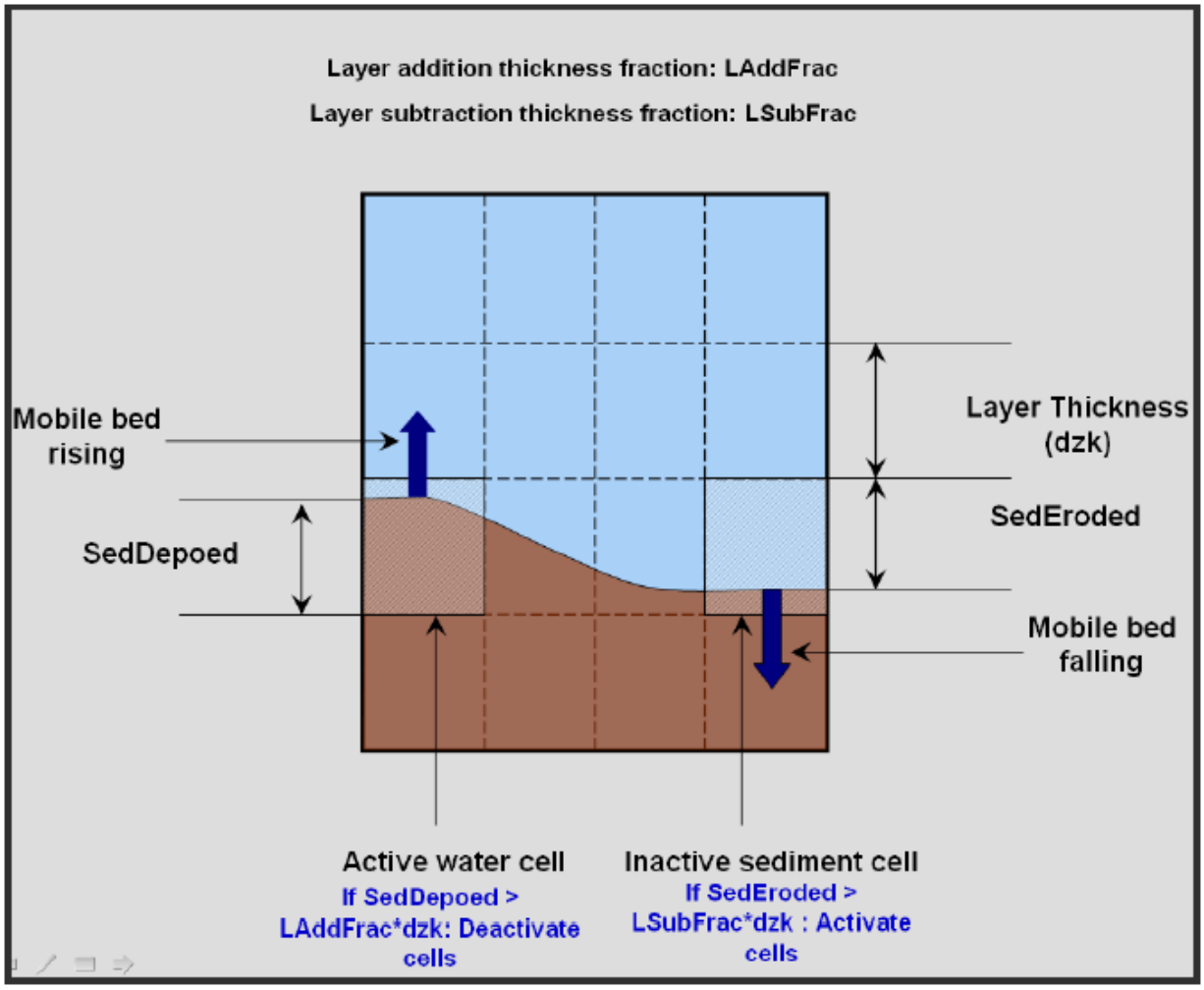

Note: LAddFrac, LSubFrac, SedDepoed etc., are the names of model variables.

The main carbon source in methanogenesis is likely the solvents used by oil sands operations. Studies have documented the microbial conversion of short chain n-alkanes (Siddique et al. 2006) and BTEX compounds (Siddique et al. 2007) to methane. Degradation was found to occur more rapidly in n-alkanes in the sequence C_{10} > C_8 > C_7 > C_6 and in BTEX compounds in the sequence toluene > xylene > ethylbenzene > benzene. Other naphtha compounds were found to be more recalcitrant within the 46-week incubation period.

Subsequent work by Siddique et al. (2008) led to first- and second-order models to predict methane production in the MLSB. This model is likely not applicable to pit lakes, because it relies on a fresh input of labile BTEX or alkanes, which will not be deposited in pit lakes after mining operations cease. However, in modelling methanogenesis in pit lakes, the "conversion efficiency (η)" coefficient described by Siddique et al. (2008) may be applicable. This coefficient, which would be determined empirically, relates the maximum amount of carbon that is reduced as a fraction of the total stoichiometric amount available. A value of 0.8 has been determined in microcosm experiments with fresh MFT (Siddique et

al. 2006, 2007); a lower value would be expected in a pit lake. Although this coefficient is not explicitly included in the OSPLM, equivalent results could be obtained by scaling down the diagenesis rate values (Section 2.3.2.3).

While the studies summarized above provide information on the nature of methanogenesis in fresh tailings, it is not clear that tailings in pit lakes will continue to produce methane at rates currently observed in the MLSB. Therefore, based on a review of the literature summarized above, the most applicable formulations for gas production appear to be the generic formulae provided by DiToro (2001). These formulae were adopted as the basis for the sediment module, as discussed by members of the OSPLM development team and the EPLMTG at the scoping stage of this project. The formulae adopted for each component of diagenesis described in the following subsections are listed in DiToro (2001), and are shown conceptually in Figure 4.

The sediment module represents the sediment bed as two layers with varying thicknesses. The upper layer, in contact with the water column, may be aerobic or anaerobic, depending on the dissolved oxygen (DO) concentration in the overlying water column and the oxygen demand exerted by the sediment bed. The thickness of the aerobic layer is calculated internally by the penetration of oxygen into the sediments. The presence of oxygen in the aerobic layer controls all oxidation processes in this layer, as described in the following subsections. Even at its maximum thickness, the aerobic layer is an insignificant fraction of the total sediment bed in terms of volume. The lower layer is always anaerobic and is the predominant source of diagenetic fluxes.

2.3.2.1 Overview of Diagenesis Module

The conceptual framework of the two-layer model adopted for OSPLM diagenesis formulation is shown in Figure 5 and Figure 6. The sediment module consists of three basic processes. The first is diagenesis (or decay) of organic matter that consists of particulate organic carbon (POC), particulate organic nitrogen (PON) and sulfate. Both PON and POC are further subdivided into different reaction classes: labile, refractory and inert. These different reaction classes are included as they have different diagenesis rates. The labile class represents rapidly decaying organic matter, the refractory class represents slow decaying organic matter and the inert class represents any fraction of PON or POC that does not participate in the diagenesis process. Inclusion of inert class is required for the mass balance of the system. The second basic process is the flux of substances produced by diagenetic processes to the upper, aerobic layer and to the water column. The third and final basic process in the aerobic layer is the oxidation process that consumes diffused oxygen from the water column exerting sediment oxygen demand (SOD) on the overlying water. There are several additional processes that take place within the sediment bed, and are discussed individually for each MFT component in the following subsections. These additional processes are not part of the standard DiToro (2001) diagenesis formulations, and have been added programmatically to the OSPLM.

The formulation adopted in the OSPLM model for diagenesis process is based on the DiToro (2001) two-layer sediment diagenesis formulation. The two-layer formulation employs an aerobic top layer and an anaerobic bottom layer. The aerobic top layer has a varying depth depending on the oxygen penetration from the overlying water column. Underneath the aerobic layer is the anaerobic layer of considerably higher thickness. The thickness of this anaerobic layer is kept constant in DiToro (2001) formulations. However, due to the nature of the OSPLM model which includes a consolidating

sediment bed, changes were made to have an anaerobic layer with spatially- and time-varying thickness. The sediment bed is thus represented using two fully-mixed sediment layers.

The two-layer sediment bed approximation is anticipated to provide useful results that clarify which parameter groups are driving fluxes. Comparisons made by DiToro (2001) of two-layer solutions to analytical solutions indicate that little information is lost by using the two-layer model. The sediment bed diagenesis model is part of a comprehensive oil sands water quality model. If a more detailed multi-layer model were adopted, the computational burden would likely be excessive with little gain in the quality of predictions.

The equations developed for the model rely on the principle of mass balance. The mass balance principle suggests that the mass of any constituents within a control volume must be the result of sources of mass to the volume, less the losses within the volume and the export from the volume. Note that the equations shown in this report assume a limitless supply of water and protons, so these are omitted from the chemical reactions and mass balances shown herein.

The mass balance equations for the two-layer model for a constituent C (concentration C_1 in aerobic layer and C_2 in anaerobic layer) are shown in Equation 1 and Equation 2.

Equation 1

$$H_1 \frac{dC_1}{dt} = J_1 + K_{L12}(C_2 - C_1) - K_{r1}C_1$$

Equation 2

$$H_2 \frac{dC_2}{dt} = J_2 + K_{L12}(C_1 - C_2) - K_{r2}C_2$$

Where H is the layer thickness, J is the production (source) flux and K_r is the decay/reaction loss for constituent C. Subscripts 1 and 2 denote the values for aerobic and anaerobic layers respectively. K_{L12} is the mass transfer coefficient between the aerobic and anaerobic layers.

The thickness of the aerobic layer is relatively much smaller than in the anaerobic layer. Due to this difference in thickness, the mass of diagenetic products within the aerobic layer is not included in the overall mass balance, although chemical conversions as constituents pass through this layer are accounted for.

Figure 5 Schematic of two-layer diagenesis model

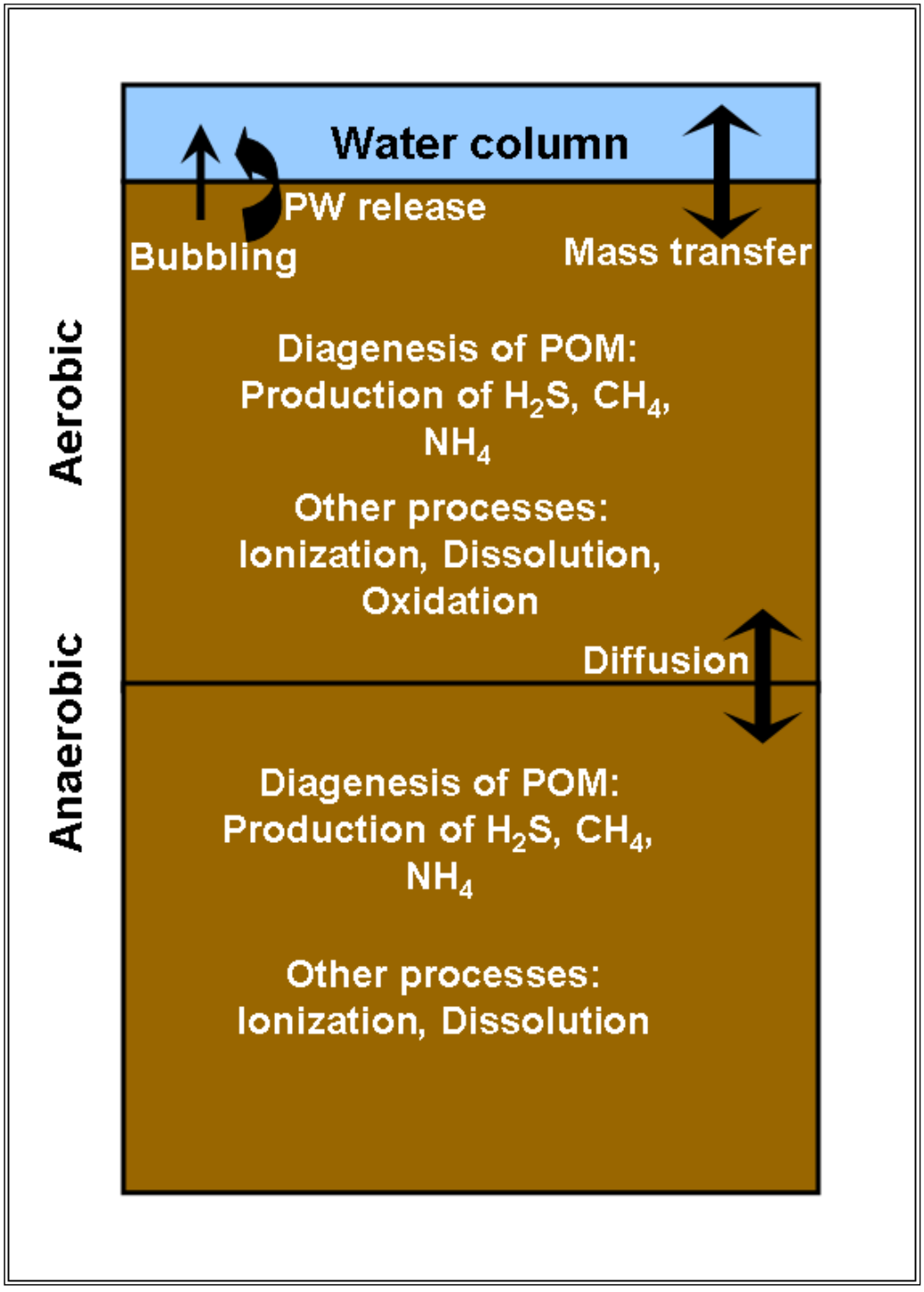

Figure 6: Diagenesis Framework

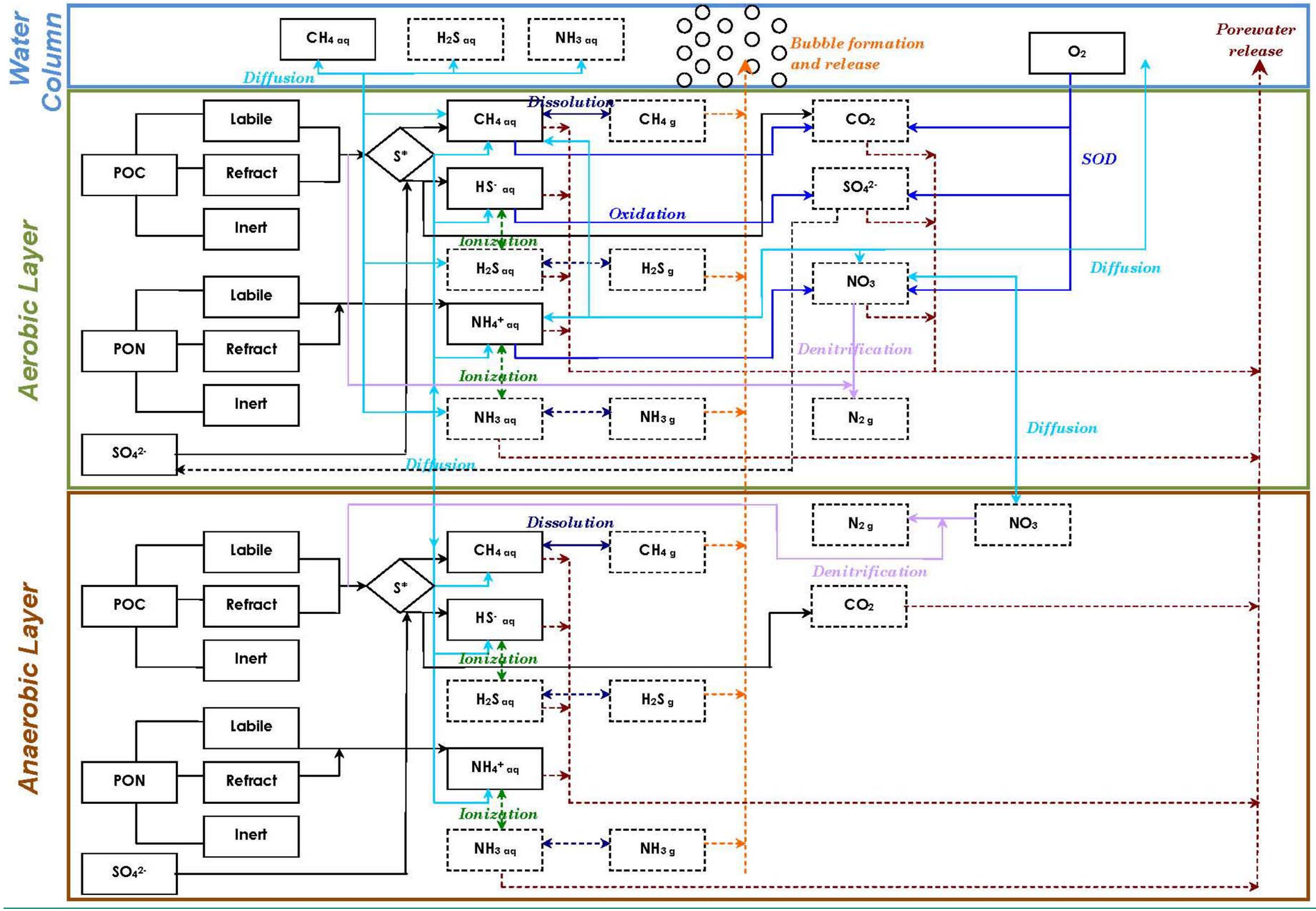

DEFINITIONS:

POC:	Particulate organic carbon
PON:	Particulate organic nitrogen
Refract:	Refractory
SOD:	Sediment oxygen demand
aq:	aqueous
g:	gaseous

2.3.2.2 Particulate Organic Nitrogen (PON)

PON in the sediment bed decreases in concentration as a consequence of mineralization (Equation 3) to ammonia (NH_3). Ammonia may be oxidized to nitrate (NO_3^-), but only in the aerobic layers where oxygen is available for the reaction. Ammonia also undergoes ionization (NH_3 to NH_4^+), depending on a user-specified pH of the pore water. Finally, ammonia may undergo dissolution ($NH_{3(g)}$ to $NH_{3(aq)}$) according to Henry's Law.

Equation 3

$$PON \xrightarrow{k_{PON}} NH_4^+$$

The mass balance equation for PON in the anaerobic layer can be given by Equation 4.

Equation 4

$$H_2 \frac{dPON_2}{dt} = -k_{PON2} H_2 PON_2$$

Where k_{PON} is the diagenesis rate. The subscript 2 denotes the anaerobic layer.

Ammonia may be transferred to the overlying water via diffusion from porewater, depending on the concentration of ammonia in the overlying water. Ammonia is similarly transferred between the aerobic and anaerobic layers, depending on the concentration gradient between the two. The mass balance equations for ammonia in the aerobic and anaerobic layers are given by Equation 5 and Equation 6.

Equation 5

$$H_1 \frac{dNH_{41}}{dt} = +k_{PON1} H_1 PON_1 - K_{L01}(NH_{40} - NH_{41}) + K_{L12}(NH_{42} - NH_{41}) - k_{NH4-1} H_1 NH_{41}$$

Equation 6

$$H_2 \frac{dNH_{42}}{dt} = +k_{PON2} H_2 PON_2 - K_{L12}(NH_{42} - NH_{41})$$

Where K_{L01} and K_{L12} are the mass transfer coefficients for ammonia at sediment-water and aerobic-anaerobic interfaces. NH_{40} is the concentration of ammonia in the overlying water column. k_{NH4-1} and k_{NH4-2} are the nitrification rates for aerobic and anaerobic layers. The nitrification reaction follows Monod kinetics (DiToro 2001) with respect to the ammonia and oxygen concentrations – the rate of nitrification decreases as the ammonia concentration increases. Similarly, the nitrification reaction decreases with the decreasing oxygen concentrations. This phenomenon can be represented by combining the two effects to modify the nitrification rate as shown in Equation 7. The same modification can be applied to the anaerobic layer.

Equation 7

$$k_{NH_{4-1}} = k_{NH_{4-1}} * \frac{K_{M,NH_4}}{K_{M,NH_4} + NH_{4-1}} * \frac{O_{2-1}}{K_{M,O_2} + O_{2-1}}$$

Where $K_{M,NH4}$ is the half-saturation constant for ammonia and $K_{M,O2}$ is the half-saturation constant for oxygen.

Figure 7: Fate Processes for PON in the Sediment Bed

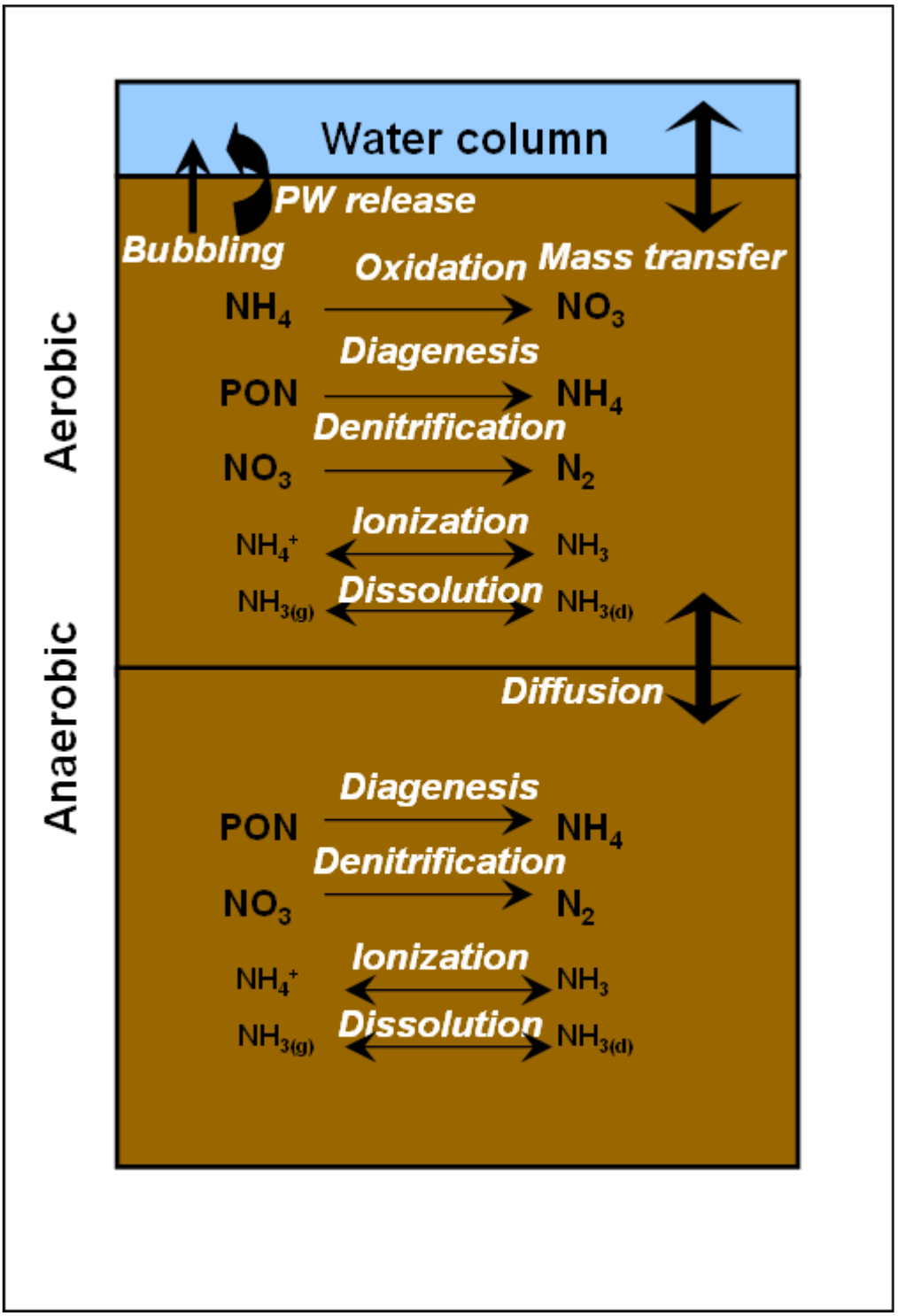

Notes: PW = pore water

Nitrate (NO_3^-) produced from the diagenesis process may be denitrified to nitrogen gas ($N_{2(g)}$) in either layer. Nitrogen gas may pass between layers and diffuse to the overlying water, depending on concentration gradients between layers. Equation 8 and Equation 9 show the mass balance for nitrate in the aerobic and anaerobic layers.

Equation 8

$$H_1 \frac{dNO_{31}}{dt} = +k_{NH4-1} H_1 NH_{41} - K_{L01}(NO_{31} - NO_{30}) + K_{L12}(NO_{32} - NO_{31}) - k_{NO3-1} H_1 NO_{31}$$

Equation 9

$$H_2 \frac{dNO_{32}}{dt} = -k_{NO_{3-2}} H_2 NO_{32} - K_{L12}(NO_{32} - NO_{31})$$

Where k_{NO3-1} and k_{NO3-2} are the denitrification rates for aerobic and anaerobic layers.

The fate process for PON is shown in Figure 7. These fate processes were programmatically included in the OSPLM. Kinematic rates and constants associated with these processes are read from the input file. A detailed description along with default values, where available, for these rates are provided in Appendix A. The OSPLM allows spatially-varying rates to provide flexibility in specifying sediment bed properties.

2.3.2.3 Particulate Organic Carbon (POC)

Methane (CH_4) is produced by the anaerobic decay of POC. In the aerobic zone, methane and oxygen combine to form carbon dioxide (CO_2) and water (H_2O). As mentioned previously, sulfate inhibition of methanogenesis has been found to occur when the sulfate concentration was above 20 mg/L (Fedorak et al. 2002). Based on these observations, a user-specified, sulfate-inhibition concentration was added to the model, with a default value of 20 mg/L of sulfate. Below this value, methanogenesis occurs (Equation 10). Above this value, consumption of POC occurs while reacting with sulfate content to form sulfide.

Equation 10

$$POC \longrightarrow CO_2 + CH_4$$

The mass balance equation for POC in the anaerobic layer can be given by Equation 11.

Equation 11

$$H_2 \frac{dPOC_2}{dt} = -k_{POC2} H_2 POC_2$$

Where k_{POC} is the diagenesis rate. The subscript 2 denotes the anaerobic layer.

Oxidation of methane may occur in the aerobic layer, which then exerts an oxygen demand on the overlying water column. Methane consumes oxygen to produce carbon dioxide (Equation 12). Transport of methane within interstitial water is through diffusion, as methane is only slightly soluble in water. When methane's solubility is exceeded in interstitial water, it forms a gas that escapes as bubbles. The relationship between the dissolved and gaseous forms is defined by Henry's Law. A similar relationship is formed for the produced carbon dioxide. Equation 13 and Equation 14 show the mass balance equations for methane in both aerobic and anaerobic layers. S_{CH4} is the methane production flux for each layer and K_{CH4} with subscripts 1 and 2 are the methane oxidation rates for the aerobic and anaerobic layers.

Figure 8: Fate Processes for POC in the Sediment Bed

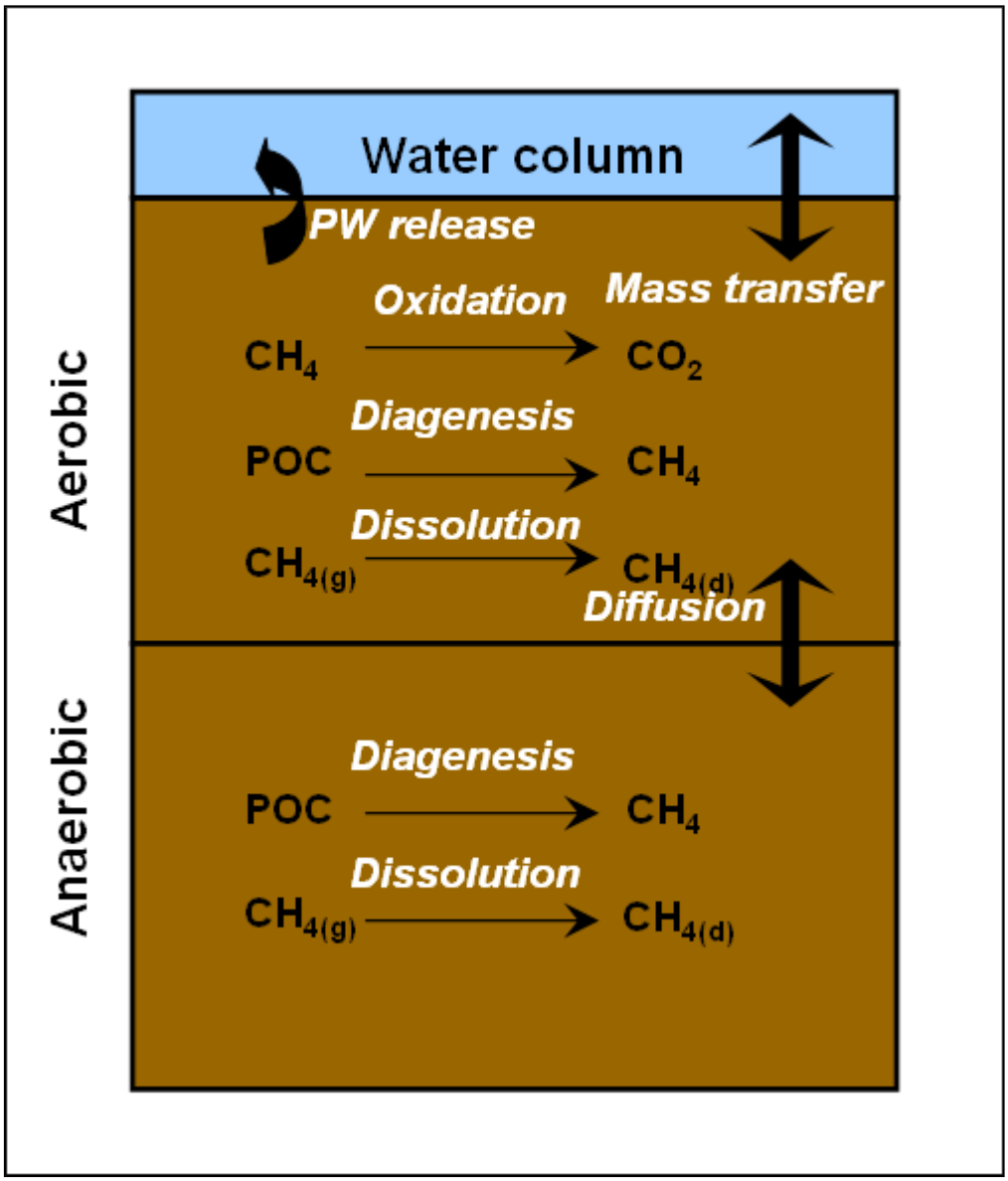

Notes: PW = pore water

Equation 12

$$CH_4 + O_2 \longrightarrow CO_2 + H_2O$$

Equation 13

$$-D_{CH_4}\frac{d^2CH_{41}}{dz^2} = -K_{CH_{4,1}}CH_{41} + S_{CH_4}$$

Equation 14

$$-D_{CH_4}\frac{d^2CH_{42}}{dz^2}=S_{CH_4}$$

Where D_{CH4} is the diffusivity of methane in the sediment bed.

Mass balance equations for both aerobic layers and anaerobic layers are formed similar to those for PON. Relationships for individual components (POC, sulfate, sulfide and methane) are developed by including all fate processes. If sulfate formation is occurring, then the sediment bed sulfate concentration increases with sulfide consumption.

The fate process for POC is shown in Figure 8. These fate processes were programmatically included in the OSPLM. Kinematic rates and constants associated with these processes are read from the input file. The OSPLM allows spatially varying rates to provide flexibility in specifying sediment bed properties.

2.3.2.4 Sulfate

Diagenesis of POC and sulfide production are competing processes, and the preference of pathway is dependent solely on the concentration of sulfate causing inhibition. Consumption of sulfate to produce sulfide is shown in Equation 15.

Equation 15

$$POC+SO_4^{2-}\longrightarrow CO_2+HS^-$$

The aerobic layer experiences oxidation of sulfide to give sulfate (Equation 16). The sulfate produced from sulfide consumption contributes to the MFT total sulfate content.

Equation 16

$$H_2S+O_2\longrightarrow H_2SO_4$$

In the OSPLM, any sulfide formed may undergo reversible ionization (HS^- to H_2S), depending on the user-specified pH of the porewater. Hydrogen sulfide can exist in both dissolved and gaseous phase.

Mass balance equations for both aerobic layers and anaerobic layers are formed similar to PON. Relationships for each individual components (sulfate and sulfide) are developed by including all fate processes. If sulfate formation is occurring, then the sediment bed sulfate concentration decreases with sulfide formation and increases with sulfide consumption.

Figure 9 shows these fate processes for sulfate in the sediment bed. Similar to previous formulations, all kinetic rates can be spatially varying in the OSPLM, as described in Appendix A.

Figure 9: Fate Processes for Sulfate in the Sediment Bed

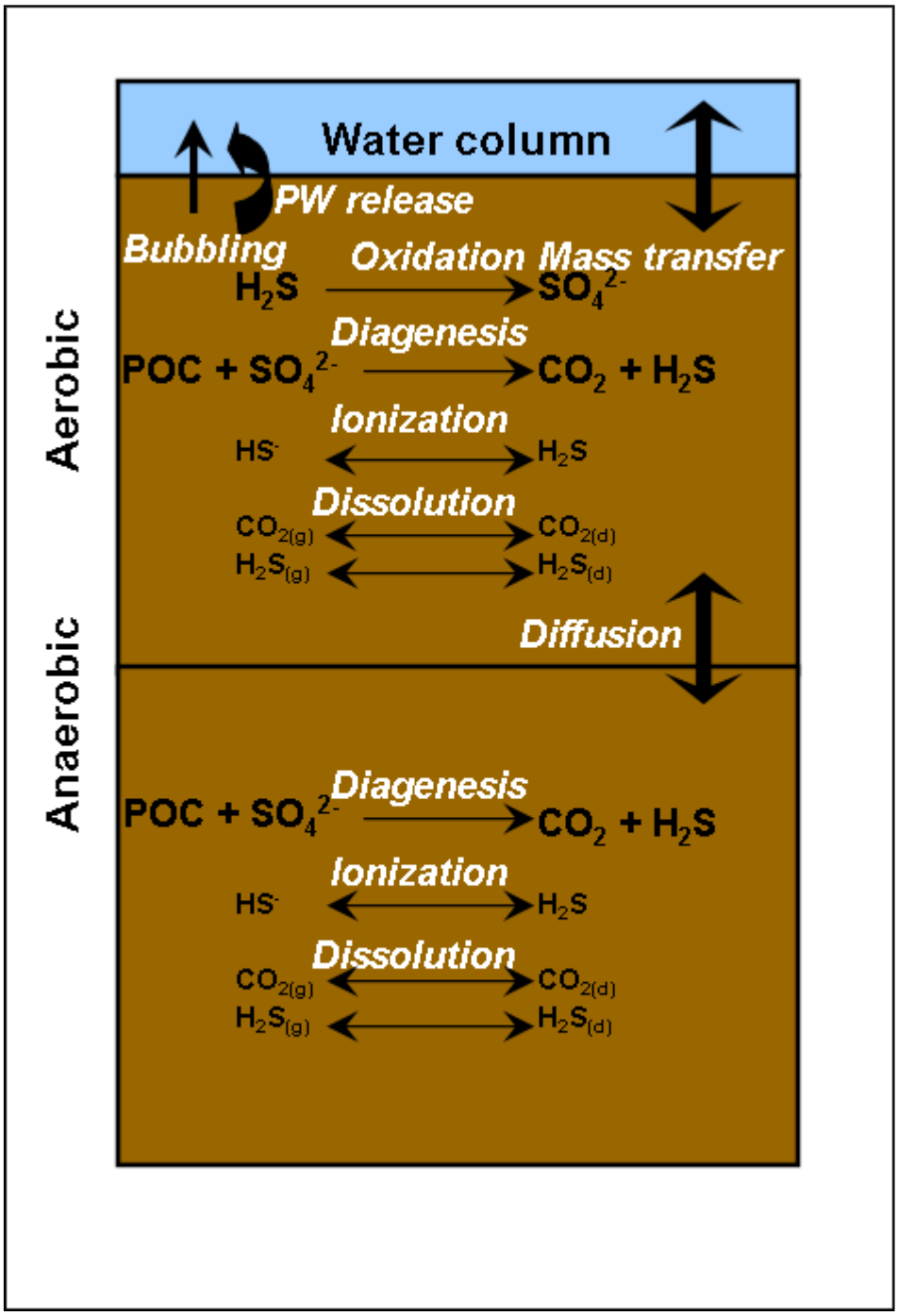

Notes: PW = pore water

2.3.2.5 Temperature correction

The rates of reactions applied in the diagenesis formulations are generally temperature dependent, and this dependence can be defined by Equation 17.

Equation 17

$$k = k_r * \theta^{(T-20)}$$

Where k_r is the reaction rate, θ is the temperature coefficient and T is the temperature.

Reaction rates in the diagenesis formulations applied in OSPLM make use of this temperature dependent relationship. Currently the temperature in the sediment bed is constant in time. However, this temperature dependence can also be applied if OSPLM is modified to calculate a time-varying sediment bed temperature.

2.3.2.6 Ionization

Diagenesis products such as sulfide and ammonia can undergo ionization based on their ionization potential and water pH. Currently the OSPLM keeps porewater pH constant with time. Future upgrades in OSPLM may calculate a time-varying pH in porewater. Ionization of ammonia in porewater occurs according to Equation 18.

Equation 18

$$NH_4^+ \leftrightarrow NH_3 + H^+$$

Under equilibrium conditions, the concentration of individual reactants and products can be written according to Equation 19

Equation 19

$$K \leftrightarrow \frac{[NH_3] * [H^+]}{[NH_4^+]}$$

Where $[H^+]$ can be defined by pH and calculated by Equation 20

Equation 20

$$pH = -\log_{10}[H^+]$$

The equilibrium constant (K) is provided as input in OSPLM as pK which is defined by Equation 21.

Equation 21

$$pK = -\log_{10}[K]$$

2.3.3 Bubbling to Surface (P5)

The physics of bubble formation and escape from sediments has not been studied in detail in oil sands pit lakes. However, multi-phase systems have been studied in the context of contaminated sites, methane hydrate recovery and greenhouse gas accounting. The results of these studies, which were reviewed to inform the development of a bubble formation framework for the OSPLM, are summarized briefly in the following subsection.

2.3.3.1 Review of Bubble Dynamics Studies

The formation of gas bubbles in sediments and release to the overlying water column is described by van Kesteren and van Kessel (2002a) in their work relating to harbour sludge. Briefly, gases (CH_4 and CO_2) are produced by methanogenesis, which increases the concentration of these gases in interstitial waters within the sediments. In fine sediments, advective and diffusive transport of gases from the interstitial waters is very slow. Therefore, additional gases being produced lead to higher dissolved gas concentrations up to the point of saturation (as determined by Henry's Law), at which point bubbles will form. Bubbles continue to grow until the upward force on the sediment exceeds the fracture energy, at which point the bubbles escape to the overlying water column.

In fine sediments, vapour pressure is reduced due to adsorption of gases to the surface of solids, and surface tension increases the pressure inside bubbles relative to ambient water. Consequently, the saturation of methane in porewater may be expressed as a function of several variables, as described in van Kesteren and van Kessel (2002a). Once the saturation point is reached, bubbles are assumed to form according to a bubble growth equation proposed by Brennen (1995) that predicts bubble diameter. Bubbles will continue to grow until they deform the surrounding matrix.

While van Kesteren and van Kessel (2002a) indicated that bubbles will form until they create cracks in the matrix, at which time the bubbles will escape the sediments, subsequent work indicated that bubbles will escape when the bulk density of the sediments is less than the bulk density of water (Kesteren and van Kessel 2002b). This latter explanation may have more relevance for MFT, which has low shear strength. Tailings have been described as MFT if the shear strength is less than 10 kPa, although a more detailed analysis indicated that aged MFT would have a shear strength of less than 50 Pa near the surface and approximately 5000 Pa near the bottom (Suthaker 1995).

Methane bubble formation in muddy marine sediments has been studied using x-ray computed tomographic images (Boudreau et al. 2005). Bubbles were found to form oblate spheroids, then fracture the sediment when internal bubble pressure rose above a critical pressure. In response to bubble growth, muddy sediment was found to act as a solid and fracture, whereas sandy sediments responded more like a fluid. Bubbles formed according to mechanics predicted by earlier work as per the Linear Elastic Fracture Mechanics (LEFM) model (Johnson et al. 2002, Gardiner et al. 2003). This LEFM model has recently been solved as a transient model using the finite-element method (Algar and Boudreau 2009) to overcome the quasi-steady state assumption from earlier work. The LEFM model predicts bubble size and growth rate as a function of methane production rate and physical characteristics of the sediment. Growth rates computed by this model were comparable to field observations from other studies (Martens and Klump 1980, Klein 2006). While the LEFM model is applicable to the micro-scale of bubble formation, and the current CEMA modelling effort is applicable to the macro-scale, the LEFM model may be of use in validating certain aspects of the bubble dynamics predicted by the CEMA model, such as overall growth rate and volume.

Bubble-facilitated transport of solid- and gas-phase contaminants has been examined in the laboratory by measuring the amount of phenanthrene transferred by bubbles from the sediment to the overlying water column in column experiments (Yuan et al. 2007). Re-suspension of total suspended solids (TSS) due to ebullition was observed but was not quantitatively measured. Yuan et al. (2009) continued this work with additional column experiments and the development of a mathematical transport model. This model was used to predict the transfer of contaminants from sediments to the water column and atmosphere. This model was developed

primarily to assess sediment capping as a mitigation measure for contaminated sediments. Based on the results of these laboratory tests, Yuan et al. (2007) concluded that bubble-mediated transport was not likely to contribute significant amounts of contaminants compared to other modes of transport such as bioturbation, at least at ebullition rates expected in nature. However, depending on the ebullition rates predicted for pit lakes, which may exceed those observed in natural systems, bubble-mediated transport of contaminants may be a dominant process, and was included mechanistically in the OSPLM.

2.3.3.2 Model Formulation of Bubble Formation and Release

Continuous production of dissolved gases (H_2S, CH_4, CO_2 and NH_3) through diagenesis may result in oversaturation, at which point bubbles may form. The relationship between the dissolved and gaseous (bubble) phase is described by Henry's Law. The solubility of each gas determines the amount of gas formed in the interstitial pores. In situ rates of bubble formation have not been measured in MFT, and thus OSPLM relies on bubble formation and growth relationships. The growth model adopted for OSPLM is based on the work of Boudreau et al. (2001a, 2001b). This model was chosen because it considers a distributed source of gas formation which is not normally included in other bubble growth models. This approach is important as the sediment bed continually produces gas through diagenesis. The authors note that the validity of the model is restricted by its assumptions but that the results are correct within an order of magnitude even if some of the assumptions are violated. A complete bubble creation and release model would include nucleation, kinetics of gas adsorption, transport of the gas, and mechanical response of the sediments. However, nucleation kinetics are ignored by assuming that there are abundant nucleation sites and that the bubbles form without hindrance. Similarly, the rate of growth of bubbles in sediments is sufficiently slow that adsorption kinetics can be ignored. This assumption leaves only transport and mechanical controls to be considered.

In order to describe the sediment bubble system, the bubble-in-a-continuum model proposed by Wheeler (1988) was adopted for inclusion in OSPLM, wherein a bubble is a discrete gaseous entity that is embedded in a sediment–porewater continuum, as in a classical diagenetic model (Boudreau 1997). The bubble is considered to be spherical. In cases where bubbles adopt other shapes (e.g., disc shaped as discussed in Gardiner et al. 2003), the present model is simply an approximation using a spherical bubble of equivalent volume. Detailed formulation of the bubble growth model is provided by Boudreau et al. (2001a, 2001b). The rate of change of bubble radius obtained from the Boudreau model is shown in Equation 22:

Equation 22

$$\frac{dR}{dt} = \frac{\varphi D}{R * C_g}\left\{\frac{SR_1^2}{6D} + \left(C_1 - C_o\right)\right\}$$

where φ is sediment bed porosity, D is diffusivity of gas in the sediment bed, R is bubble radius, C_g is concentration of gas in the bubble, S is gas production rate, R_1 is a calibration parameter, C_1 is concentration of dissolved gas at a distance farther away from the site of nucleation (background concentration) and C_0 is concentration of dissolved gas at the bubble surface.

Using Equation 22, a relationship can be obtained for use in OSPLM where the bubble radius is calculated at each time step. The relationship is shown in Equation 23:

Equation 23

$$R_b^{n+1} = R_b^n + \frac{\varphi D}{R_b^n * C_g}\left\{\frac{SR_1^2}{6D} + (C_1 - C_o)\right\}\Delta t$$

where R_b^{n+1} is bubble radius at time step n+1, R_b^n is bubble radius at time step n and Δt is time step.

The concentration of gas (C_g) and the dissolved concentration at the bubble surface are always in equilibrium and are related by the Henry's Law as shown in Equation 24:

Equation 24

$$C_g = C_0 / K_i$$

where K_i is the equilibrium constant for gas "i", shown in Equation 25:

Equation 25

$$K_i = H_i /(RT)$$

where H_i is Henry's constant for gas "i", R is the universal gas constant and T is temperature in Kelvin.

Bubble growth in an elastic medium such as MFT that is susceptible to fracture occurs in two different ways (phases, Gardiner et al. 2003). If the internal gas pressure is lower than the critical value given by the strength of the material, then the bubble will expand as it receives gas by diffusion from the surrounding porewater; i.e., the sediment will compress elastically as pressure builds in the bubble (the elastic phase). When the internal pressure exceeds the strength of the sediment, the sediment will fracture and the gas bubbles will be released. The critical pressure at which bubbles result in sediment fracture (crack formation) is given by Equation 26 based on Gardiner et al. (2003):

Equation 26

$$P_{crit} = \frac{\pi^{4/5} K_{1c}^{6/5}}{24^{1/5}(E * V)^{1/5}} + P_o$$

where K_{1c} is the critical stress intensity factor and E is Young's modulus, V is bubble volume and P_0 is the background pressure.

Existing models do not consider the closing of these cracks under pressure from the overlying water column. To address this shortcoming, the formed cracks in the sediment bed are closed at a fraction of the critical pressure. The fraction is user-defined and can be used as a calibration parameter. Once the cracks close, the bubbles are not released and the bubble pressure starts to increase again until the cracks reoccur.

2.3.3.3 Bubble Growth Algorithm

This section describes the algorithm applied to calculate bubble growth and release. There are several assumptions that are applied to the following algorithm: The main assumptions are as follows:

- Gas bubbles are spherical. This assumption is adopted because the equations for the growth of disc shaped bubbles are not complete; that is, the current research is not able to define the complete fate process of bubbles.

- Gas bubbles are only released when cracks occur in the sediment bed.
- Cracks that appear in the sediment bed close when bubble pressure drops below a fraction of crack formation pressure. This fraction is user defined and can be used as a calibration parameter.

The following text describes the algorithm adopted for the OSPLM. First, the known variables are defined, as follows:

- Sediment bed porosity: φ
- Sediment bed volume: V
- Volume of porewater in sediment bed: $V_w = V^* \varphi$
- Porewater temperature: T
- Molecular weight for a gas: M_w
- Gas constant: R
- Henry coefficient for a gas: H
- Henry constant: K = H/RT
- Time step for the model computations: Δt
- Diffusion coefficient: D
- Calibration parameter: R_1
- Initial bubble radius: $R_o = 0$
- Gas source (production): S

These known variables, along with the bubble growth equations, are used to compute unknown variables:

- Concentration of dissolved gas at bubble surface: C_o
- Total concentration of gas produced: C_{tot}
- Concentration of gas in bubbles: C_g
- Concentration far away from bubble: C_1 (assumed to be equal to C_{tot} initially and C_o for the remaining simulation period)
- Bubble radius: R_b
- Background pressure: P_o
- Critical pressure for crack formation: P_{crit}
- Bubble pressure: P_{bubble}

Calculation of these unknown variables at the beginning of the simulation is done using Equation 27 to Equation 37, shown at the end of this list:

- Compute C_{tot}/C_{init} from initial production
- Calculate C_o and C_g from C_{tot} using Equation 27 and Equation 28
- Calculate Radius (R_b) using Equation 29. Assume no source (S = 0) and $C_1 = C_{tot}$
- Calculate the volume of each bubble (V_b, Equation 30), total mass (M_T, Equation 31), dissolved mass (M_D, Equation 32) and number of bubbles (N_b, Equation 33)
- Calculate critical pressure for crack formation using Equation 34
- Calculate bubble pressure using Equation 35

After the initial conditions are calculated, bubble growth and release are done using the following steps:

- Calculate new C_{tot} based on source (gas production rate) using Equation 36
- Recalculate C_o and C_g from C_{tot}/C_{init} using Equation 27 and Equation 28
- Assume background concentration is the same as dissolved concentration $C_1 = C_o$
- Calculate new radius (R_b) using Equation 37
- Recalculate the variables in Equation 30 to Equation 35
- If $P_{bubble} > P_{crit}$ then release $N_{b\text{-released}}$ bubbles to lower N_b*V_b
- Continue releasing bubbles until $P_{bubble} > P_{close}$ where P_{close} = Factor*P_{crit} and “Factor” is a user input.
- Once $P_{bubble} < P_{close}$ crack closes and no bubbles are released
- Continue till C_g increases to the point where $P_{bubble} > P_{crit}$. Repeat last four steps

The following equations based on Boudreau et. al (2001a) were used and have been discussed in the previous section. Note that volume computation (Equation 30) and mass computation (Equation 31, Equation 32 and Equation 33) equations are based on standard volumetric and mass equations.

Equation 27

$$C_o = C_{tot}/(1+K)$$

Equation 28

$$C_g = KC_o$$

Equation 29

$$R_b = \left[\frac{2\varphi D}{C_g}\left\{\frac{SR_1^2}{6D} + (C_1 - C_o)\right\}\Delta t + R_o^2\right]^{1/2}$$

Equation 30

$$V_b = \frac{4}{3}\pi R_b^3$$

Equation 31

$$M_T = C_{tot} * V_W$$

Equation 32

$$M_D = C_o * V_W$$

Equation 33

$$N_b = \frac{M_T - M_D}{V_b * C_g}$$

Equation 34

$$P_{crit} = \frac{\pi^{4/5} K_{1c}^{6/5}}{24^{1/5}\left(E * N_b * V_b\right)^{1/5}} + P_o$$

Equation 35

$$P_{bubble} = \frac{C_g RT}{M_w}$$

Equation 36

$$C_{tot}^{n+1} = C_{tot}^{n} + S * \Delta t$$

Equation 37

$$R_b^{n+1} = R_b^n + \frac{\varphi D}{R_b^n * C_g}\left\{\frac{SR_1^2}{6D} + \left(C_1 - C_o\right)\right\}\Delta t$$

2.3.3.4 Bubble-induced Turbulence

While many studies have been carried out to understand bubble-induced turbulence, our knowledge is still insufficient for developing accurate models on the effects of bubbles on turbulence properties in bubbly flows (Hosokawa and Tomiyama 2010). The addition of turbulence resulting from gases bubbling from the sediment bed is based on the two-phase bubbly flow algorithms used in modelling industrial processes of gas exchange in chemical reactors, aeration tanks and heat exchangers. To model such processes, a multi-phase calculation would need to be adopted in which two separate fluid phases (water and gas) are considered. Inclusion of such an approach is beyond the scope of current effort as it would require re-development of the fundamental structure of W2. However, a simplified correction that accounts for bubble-induced turbulence based on the turbulence viscosity (Hosokawa and Tomiyama 2010) has been adopted for the OSPLM. This correction is described below.

The momentum equation used in W2 is shown in Equation 38:

Equation 38

$$\frac{DU}{Dt} = -\frac{\nabla P}{\rho} + \nabla \nu_t (\nabla U) + g$$

where *P* is the pressure, *ρ* is the density of water, *U* is the velocity vector (u, v and w in the direction of x, y and z axis) and *g* is the acceleration due to gravity.

v_t, which is the turbulent viscosity, can be modified to include the bubble-induced turbulence. The net turbulent viscosity in a bubbly flow can be calculated using Equation 39:

Equation 39

$$\nu_{net} = \nu_t + \nu_b$$

where v_b is the bubble-induced turbulence that can be given by Equation 40.

Equation 40

$$\nu_b \propto d_b \times V_R$$

Where d_b is the average bubble diameter and V_R is the average rise velocity. A scaling factor (φ) is added to obtain a relationship to calculate bubble-induced turbulence as shown in Equation 41.

Equation 41

$$\nu_b = \varphi \times d_b \times V_R$$

2.3.3.5 Bubble Rise and Release

Once the bubbles are released into the water column, they rise due to the buoyancy forces acting on them. Due to the wide range of possible gas bubble sizes rising from the sediment bed, the more general formulations of Zheng and Yapa (2000) were adopted for use in OSPLM. Although spherical bubbles are modeled in the OSPLM, the rise velocity computations from Zheng and Yapa (2000) are also applicable to non-spherical bubbles. In the case of non-spherical bubbles, an equivalent spherical diameter (d_e) for the bubble is used. The following equations show the calculation of rise velocity (V_r) and have been taken directly from Zheng and Yapa (2000).

For bubbles of small size range ($d_e \leq 1$ mm)

Equation 42

$$V_r = \frac{R\mu}{\rho d_e}$$

where *μ* is the dynamic viscosity of gas, *ρ* is the density of water and *R* is the Reynolds number (Table 2).

For bubbles of intermediate size range (1 mm < d_e ≤ 15 mm)

Equation 43

$$V_r = \frac{\mu}{\rho d_e} M^{-0.149(J-0.857)}$$

Equation 44

$$H = \frac{4}{3} E_o M^{-0.149} \left(\frac{\mu}{\mu_w} \right)^{-0.14}$$

Equation 45

$$M = g\mu^4 \Delta\rho / \rho^2 \sigma^3$$

Equation 46

$$E_o = g\Delta\rho d_e^2 / \sigma$$

Equation 47

$$J = 0.94 H^{0.757} \text{ when } 2 < H \leq 59.3$$

Equation 48

$$J = 3.42 H^{0.441} \text{ when } H > 59.3$$

H, M, E_o and *J* are intermediate velocity calculation variables, and *σ* is the interfacial tension.

For bubbles of large size range (d_e > 18 mm)

Equation 49

$$V_r = 0.711\sqrt{g d_e \Delta\rho / \rho}$$

Rise velocity for bubbles between the size of 15 mm and 18 mm is calculated by linearly interpolating between the rise velocity at 15 mm using Equation 43 and 18 mm using Equation 49. Reynolds number (R) for bubbles can be calculated using formulations given in Table 2.

Table 2: Formulae Used to Determine Reynolds Number (Zheng and Yapa 2000)

Range	Reynolds number formula
$N_D \leq 73$	$R = \frac{N_D}{24} - 1.7569X10^{-4} N_D^2 + 6.9252X10^{-7} N_D^3 - 2.3027X10^{-10} N_D^4$
$73 < N_D \leq 580$	$\log R = -1.7095 + 1.33438W - 0.11591W^2$
$580 < N_D \leq 1.55X10^7$	$\log R = -1.81391 + 1.34671W - 0.12427W^2 + 0.006344W^3$
$N_D = 4\rho\Delta\rho g d_e^3 / 3\mu^2$ and $W = \log N_D$	

The bubbles exchange gases with the water column during their transit through the water column. Once the bubbles rise to the water surface, a burst factor is applied that represents the bubbles bursting and releasing gases to the atmosphere. The same factor controls the duration of the bubbles in the water column.

The exchange of gases between the bubbles and the water column is calculated using a gas transfer coefficient. The equilibrium dissolved concentration for the gases are calculated for the bubbles based on Henry's Law, as per Equation 50:

Equation 50

$$C_{Eqb-d-i} = C_{bubble-i} / K_i$$

Where $C_{Eqb-d-i}$ is the equilibrium concentration in dissolved phase for gas "i" in the bubble, $C_{bubble-i}$ is the concentration in gaseous phase for gas "i" in the bubble and K_i is the equilibrium constant for gas "i"

Flux of gas from bubble to water for gas "i" is obtained through Equation 51:

Equation 51

$$J_{g-w-i} = K_{g-w-i}(C_{Eqb-d-i} - C_{d-i})$$

where K_{g-w-i} is the gas transfer coefficient for gas "i" and C_{d-i} is the dissolved concentration of gas "i".

2.3.4 Unconsolidated Sediment Resuspension/Erosion (P6 and P7)

The unconsolidated sediments in the sediment bed can experience resuspension and resettling from the water column. The process is added to the original W2 code based on the resuspension formulations used in sediment transport models. User specification of sediment types (cohesive or non-cohesive) defines the type of resuspension formulation adopted. The following subsections will discuss these formulations separately.

2.3.4.1 Cohesive Sediments

Cohesive bed erosion occurs in two distinct modes, mass erosion and surface erosion (Tetra Tech 2002). Mass erosion occurs rapidly when the bed stress exerted by the flow exceeds the shear strength, τ_s, of the bed. Surface erosion on the other hand occurs gradually when the flow-exerted bed stress is less than the bed shear strength but greater than a critical erosion or resuspension stress, τ_e, which is dependent on the shear strength and density of the bed. Typically, under accelerating flow resulting in increased bed stress first gradual surface erosion takes place, followed by mass erosion. If the bed is well consolidated then only surface erosion will take place. The two erosion types and their critical stresses are given in Equation 52 and Equation 53 below.

Equation 52

$$\tau_s = a_s \rho_b + b_s$$

where ρ_b is the bed bulk density and a_s is 9.808 and b_s is -9.934 for bed bulk density greater than 1065 kg/m^3 (Hwang and Mehta 1989). The bed is considered fluidized below 1065 kg/m^3 and thus not considered erodible.

Equation 53

$$\tau_e = a(\rho_b - 1.065)^b + c$$

where ρ_b is the bed bulk density in gm/cm^3 and *a* is 0.883, *b* is 0.2 and c is 0.05.

When bed shear is greater than surface stress than the surface erosion occurs. Under increased bed shear, the mass erosion shear stress may be exceeded when the mass erosion overtakes surface erosion. At this point mass erosion occurs. The scour during these erosions is given by Equation 54.

Equation 54

$$\log_{10}(F_{Sed-i}) = 0.23\exp\left(\frac{0.198}{\rho_b - 1.0023}\right)$$

2.3.4.2 Non-cohesive Sediments

The non-cohesive sediment particles that settle from the water column accumulate on the sediment bed. Under the influence of moving water and its shear exerted on these bed sediments, the particles experience an uplifting force which, if greater than critical shear stress for erosion, moves the particles back into the water column. OSPLM quantifies the non-cohesive sediment erosion based on the formulation of van Rijn (1984). The erosion is modelled as the diffusive flux of sediments into the water column. This diffusive flux is computed based on estimating the bed concentration ($C_{a\text{-}Sed\text{-}i}$) and near-bed concentration ($C_{a+\Delta a\text{-}Sed\text{-}i}$).

The bed concentration is estimated using Equation 55 (van Rijn 1984).

Equation 55

$$C_{a-Sed-i} = 0.015\frac{D_{Sed-i}}{a} * \frac{T_{Sed-i}^{1.5}}{D_{Sed-i}^{0.3}}$$

The near-bed concentration can be estimated by linearly interpolating the suspended sediment column concentration or by applying the formulation of Jones and Lick (1999) shown in Equation 56.

Equation 56

$$C_{a+\Delta a-Sed-i} = C_{a-Sed-i} * Exp\left(-\frac{w_{s-Sed-i} * \Delta a}{0.067 * Depth * u_*}\right)$$

Using the above two transport exchange processes, the source/sink term for i-th size class sediment is written as follows:

Equation 57

$$F_{Sed-i} = \left[w_{s-Sed-i} * C_{Sed-i}\right] - \left[D_v \frac{C_{a+\Delta a-Sed-i} - C_{a-Sed-i}}{\Delta a}\right]$$

D_v is the vertical diffusion and is given by:

Equation 58

$$D_v = \beta\varphi A_v$$

Equation 59

$$\beta = 1 + 2 * \left(\frac{W_S - Sed - i}{u_*}\right)^2 \quad \text{for} \quad 0.1 < \frac{W_S - Sed - i}{u_*} < 1$$

φ is the factor accounting for the damping in the particle movement due to the net sediment concentration and is given by:

Equation 60

$$\phi = 1 + \left(\frac{C}{C_o}\right)^{0.8} - 2 * \left(\frac{C}{C_o}\right)^{0.4}$$

where C is the net volumetric concentration of sediments and C_O (= 0.6) is the maximum volumetric concentration. A_v is the vertical diffusion coefficient computed internally by W2.

2.3.5 Non-algal Water Clarity (P8)

Water clarity or turbidity is an indicator of the amount of sediment and related constituents within a waterbody. Relationships between TSS and turbidity can be developed based on site-specific data. TSS includes both suspended sediment and organic material in a water sample. The relationship between TSS and turbidity is usually considered to be linear on a natural logarithmic scale (Packman et al. 1999). A generic relationship for the two entities is given by Equation 61:

Equation 61

$$\ln(Turbidity) = A_{turb} \ln(TSS) + B_{turb}$$

Both A_{turb} and B_{turb} are site-specific parameters. The same relationship was applied for the OSPLM. The TSS concentrations are calculated internally in the model and, based on the values of A_{turb} and B_{turb}, turbidity values are calculated in Nephelometric Turbidity Units (NTU).

2.3.6 Oxygen Consumption by Released Gases (P9)

In the aerobic zone of the sediments and water column, it is assumed that methane will be oxidized if conditions are suited to methanotrophs.

A confounding factor in predicting methane oxidation is the presence of ammonia, which can stimulate methane oxidation at low levels (Jones and Morita 1983) and inhibit it at high levels (Ward and Kilpatric 1990). Ammonia or other nitrogen compounds are necessary as a nitrogen source for bacterial growth, so methane oxidation may not occur below certain concentrations of ammonia. However, high concentrations of ammonia may also inhibit methane oxidation due to one of the following processes:

- methanotrophs switching to oxidizing ammonia when ammonia reaches certain levels (Boeckx and van Cleemput 1996);
- methanotrophs becoming outcompeted by nitrifiers (Cai and Yan 1999); or
- toxicity of ammonia or byproducts of its oxidation (King and Schnell 1994).

Methane oxidation has been found to occur in narrow bands within the thermocline due to the dependence of methanotrophs on an oxygen-sensitive nitrogen fixation process (Bédard and Knowles 1997, Harrits and Hanson 1980, Rudd et al. 1976, Utsumi et al. 1998a). In these studies, most methane was oxidized at this oxic/anoxic interface. Following lake turnover, the methanotrophs were able to oxidize methane throughout the water column, which was attributed to ammonia entering the epilimnion from the hypolimnion. Once the ammonia had been consumed in the epilimnion, high oxygen concentrations precluded nitrogen fixation, which in turn precluded methane oxidation (Rudd et al. 1976). Other studies have found that the majority of methane oxidation occurs near the sediment water interface in a narrow zone between the aerobic and anaerobic layers (Harrits and Hanson 1980, Kelley 2003).

Methane oxidation was also dependent on DO concentrations, with the highest rates of oxidation occurring at less than 1 mg/L DO (Rudd et al. 1976). However, a half-saturation constant for methane oxidation has been estimated at 0.5 to 0.8 mg O_2/L in Lake Washington, which would lead to maximum oxidation occurring at DO > 1 mg/L (Lidstrom and Somers 1984), although methane oxidation occurred mainly in the top 5 mm of sediment in this lake throughout the year.

Despite the findings of the studies mentioned above, others have found methane oxidation to be relatively insensitive to these factors (Utsumi et al. 1998b). Utsumi et al. (1998b) examined sediment methane production and water column methane oxidation in a lake with a large surface area and relatively shallow depth. The hydrodynamics in this lake, which mixed frequently and was therefore generally oxic throughout, may be representative of a shallow pit lake such as Base Mine Lake, at least during the open water season. Over a five-year period, methane oxidation rates in this lake were found to vary seasonally by two to three orders of magnitude, with lows occurring in winter and highs in fall. Methane oxidation rates were not related to temperature, nor to concentrations of methane, DO or dissolved inorganic nitrogen.

Umorin (2002) constructed a mathematical model of methane oxidation that considered substrate concentrations according to the Michailis-Menten equation and inhibition by dissolved forms of inorganic nitrogen and oxygen. The model results, which agreed with experimental data from column tests, indicated that ammonia produced by protozoa was the main factor inhibiting methane oxidation. When inhibitory competition was removed from the model, methane oxidation rates increased under given concentrations of phosphorus and nitrogen.

The majority of studies indicate that inorganic nitrogen is necessary at low levels to provide a nitrogen source for bacteria, and that ammonia may inhibit methane oxidation at high levels. However, there is no clear consensus on the inhibitory process, or the level at which this may occur. Furthermore, nitrifiers have also been found to oxidize methane (Bédard and Knowles 1989), and methanotrophs have been found to co-oxidize ammonia (Harrits and Hanson 1980). Given the uncertainty as to the behaviour of methanogens and nitrifiers in oil sands pit lakes, it is recommended that this inhibition concentration be determined experimentally through studies such as the one being conducted by Dr. Weisener at the University of Windsor. Until such a study is conducted, it is proposed that the OSPLM assumes first-order kinetics for methane oxidation in the water column. Depending on the results of future studies, a site-specific ammonia inhibition concentration, above which methane oxidation does not occur, may be added to the model at a later date.

First-order rates of methane oxidation have been reported in several studies from various lakes and reservoirs world-wide, and some examples are provided in Table 3.

Table 3: Literature Values on First Order Methane Oxidation Rates

Lake/Reservoir	Specific Methane Oxidation Rates (d^{-1})	Reference
Lake St. George	0.02 – 3	Bédard and Knowles (1997)
Petit-Saut Reservoir	4.13	Dumestre et al. (1999), cited in Guérin and Abril (2007)
Petit-Saut Reservoir	2.64	Guérin and Abril (2007)
Gulf of Mexico	0 – 0.76	Kelley (2003)
Lake Kevaton	0.45 – 3.43	Liikanen et al. (2002), cited in Guérin and Abril (2007)
Lake 120 (ELA)	0.9 – 1.25	Rudd et al. (1974), cited in Guérin and Abril (2007)
Lake Constance	0.33 – 0.71	Schmidt and Conrad (1993), cited in Guérin and Abril (2007)
Minnesota Lakes	0.43	Striegl and Michmerhuizen (1998), cited in Guérin and Abril (2007)
Lake Kasumigaura	0.012 – 3.0	Utsumi et al. (1998b)
Lake Nojiri	0.1 – 1	Utsumi et al (1998a), cited in Guérin and Abril (2007)
ELARP pond	0.36 – 2.4	Venkiteswarran and Schiff (2005), cited in Guérin and Abril (2007)
FLUDEX reservoirs	0.58 – 1.03	Venkiteswarran and Schiff (2005), cited in Guérin and Abril (2007)

2.3.7 Chemical Oxygen Demand (P10)

This process is modelled using the standard W2 formulation described in Cole and Wells (2008).

2.3.8 Biological Oxygen Demand (P11)

In the water column, this process is modelled using the standard W2 formulation described in Cole and Wells (2008). In the sediment layer, generic BOD constituents may be added in a similar fashion to how they are added and modelled in W2. As the generic BOD constituents are released from the sediment layer, they will be internally linked to W2 and they will exert a BOD in the water column. Naphthenic acids are an example of a generic BOD constituent that may be added to the OSPLM sediments and water column.

2.3.9 Variable Lake-bottom Oxygen Consumption (P12)

This process is modelled using the standard W2 formulation described in Cole and Wells (2008). In addition, the pore water and gases released from the gas production module exert additional sediment oxygen demand, which results in variable lake-bottom oxygen consumption. Consumption of oxygen due to gas formation is described earlier in Section 2.3.2.

2.3.10 Fluid Fine Tails Layer (P13)

In lakes that contain MFT, overlying the MFT bed is a gel-like layer of fine tailings that may act as a barrier between the MFT bed and the water column. This layer, termed the Fluid Fine Tails (FFT) layer, has been added to the OSPLM to account for phenomena observed at waterbodies at Syncrude's Mildred Lake operation. The FFT layer is essentially an unconsolidated layer of very fine material suspended at the upper boundary between the MFT-water interface.

The FFT layer was incorporated in the OSPLM by adding a water layer with very high TSS concentration (~30% solids w/w). This layer has a high density that keeps it near the bottom of the water column, suspended over the MFT bed. This behaviour was modelled by using a separate and near-zero settling velocity in the FFT layer. Overall, suspended sediments in the water column settle to the FFT layer, in which settling occurs at a much

lower rate. Due to high density gradient between the FFT layer and the remaining water column, there is reduced mass transport between the two media.

Within the model, the FFT layer can be made to disappear with time in one of two ways: First, a user-defined period can be selected to turn the layer off. Second, a settling rate of TSS from the FFT layer to the MFT bed can be introduced. With the second approach, the TSS will gradually settle out and the FFT layer will lose its high TSS concentration.

The settling rate of material in the FFT layer is not presently known, although it is known that this rate is very slow. Therefore, field or laboratory studies should be conducted to determine whether this layer will be present in a pit lake that has not received fresh tailings in several years to decades (the typical filling period for oil sands pit lakes after mine closure). To account for this uncertainty, and to overcome potential model instability due to the sharp boundary density boundary between the FFT layer and the overlying water cap, the FFT layer may be switched off by the user. Additionally, the FFT layer is automatically switched off immediately prior to the addition of new bottom layers being added to the model grid during consolidation to overcome stability issues.

2.3.11 Salt Rejection (P14)

The process of salt rejection was incorporated into W2 in the Phase II Model as described in CEMA (2007). Since that time, improvements to the W2 ice module were made as part of release v.3.6. In addition, ice calibration has been completed using the W2 model for several compensation lakes in the Oil Sands Region (e.g., Shell 2009). These lakes were modelled for No Net Loss plans, where ice thickness and ice-cover duration were the focus of additional calibration due to their potential effects on late-winter DO concentration. For these modelling projects, W2 “detailed” ice module coefficients were adjusted to obtain a match with regional lakes, as described in Appendix D, of Shell (2009). However, salt rejection was not included programmatically, but rather, was set prescriptively through external time series files.

For the OSPLM, salt rejection is included mechanistically as part of the detailed ice module, without the need for external files. Salt rejection is included by removing 0.917 units of water from the top layer for every unit of ice formed to account for differences in density.

The ice module was also configured to trap bubbles under the ice. During the ice-cover period (as predicted by the detailed ice cover module), bubbles are not allowed to escape, and remain effectively bound at the upper surface of the water column where they can interact with aqueous constituents. Once the ice melts, the bubbles are assumed to be released to the atmosphere.

3.0 RECOMMENDATIONS

As discussed in Section 1.3, the present stage of model development is experimental, and future refinements of the model are anticipated. Refinements have been suggested by the model developers and by CEMA reviewers, and have been classified according to priority.

3.1 Near-term recommended updates

The present model includes a framework for predictive modelling of sediment diagenesis and gas production in an oil sands pit lake. The model has been developed to account for the processes described in Section 2. In the next phase of development, the following processes are recommended for addition:

i) Linkage of gases produced in the sediment to oxygen consumption in the water column. Presently, ammonia is the only substance that is produced in the sediment module and exerts an oxygen demand in the water column by standard W2 formulations. A separate module should be developed to create an oxygen demand based on methane and sulphide concentrations. Note that functionality has been added to link dissolved CBOD flux from the sediment to CBOD groups in the water column.

ii) Consumption of oxygen due to sediment resuspension. Oxygen may be consumed by degradation of chemicals adsorbed to suspended sediments. The oxygen consumption model did not account for this oxygen demand. The oxygen consumption module can be modified to include a relationship estimating additional oxygen demand from sediment resuspension. Estimating this relationship may be challenging, because the demand may be both site-specific and time-varying.

iii) Dynamic calculation of sediment pH and temperature. The processes described in Section 2 will affect the pH of the sediments and pore water, which may in turn affect chemical reactions through Le Chatelier's principle. This feedback loop should be included in the sediment module by calculating pH. In addition, the model should be able to read a time-varying sediment temperature timeseries.

iv) Incorporate metal diagenesis. Cycling of metals, such as iron and manganese, as well as the binding of these metals with sulphides and other anions should be considered in future updates.

3.2 Medium-term refinements to address limitations

There are limitations to the model framework where simplifying assumptions needed to be made. The need for these assumptions arose due to various issues, such as lack of complete numerical models available for some processes or excessive computational effort required for others. These assumptions are not anticipated to prevent the model from achieving CEMA's objectives, either because they exert a small influence on lake water quality or because they may be accounted for through calibration parameters or direct time series inputs. Therefore, these are considered lower priority refinements that should be addressed as the opportunity arises.

i) Mechanistic consolidation of tailings. Rather than reading a time series that specifies tailings consolidation, a module could be developed to calculate this process internally. Ideally, this model would include the feedback loop of methanogenesis influencing consolidation rates.

ii) Effect of bubbles on ice formation. Bubbles released from the sediment bed can affect ice formation. The ice formation is estimated in OSPLM using the W2 ice formation model. Ideally, the model should include any changes in ice formation due to the gas bubbles reaching the water surface.

iii) Nucleation of gas bubbles. Presently, the model needs an initial estimate of gas bubbles, and new bubbles will not form if diagenesis stops completely and then restarts.

iv) Vertical variation in sediment properties. It is anticipated that calibration will focus on the active zone of tailings processes, so this refinement is listed for consideration but is low priority.

3.3 Long-term recommendations to validate the model

Regardless of which refinements listed in Sections 3.1 and 3.2 are completed, the following steps are recommended to validate the model framework and ultimately set up a predictive model:

i) Obtain reasonable estimates, where available, for all applicable processes and characteristics (e.g., gas production rates, dissolved gas concentrations, dissolved constituent concentrations). The primary source of this information would be tailings ponds or experimental reclamation waterbodies on existing oil sands operations. Other potential sources of information are EIAs for concentrations and literature sources for process rates in natural, impacted and constructed waterbodies. This step was partially completed while conducting the literature search to identify relevant algorithms; any values encountered during this search were documented in Section 2.

ii) Configure a preliminary model application based on available rates and coefficients to systematically test performance. Run the model and examine rates for all applicable processes and concentrations of each constituent. Compare the computed rates and concentrations to expected values, and attempt to calibrate the model to an "order of magnitude" level. Verify that the model responds as expected to changes in inputs. Identify any areas where reasonable rates cannot be predicted by the model, or where coefficients must be set outside of expected ranges to obtain reasonable results.

iii) If any processes cannot be replicated in the model using reasonable rates and coefficients, alternate formulae may need to be incorporated into the model. The literature sources documented in Section 2 provide alternate sources of formulae for several processes.

iv) After the model framework has been validated, laboratory and field studies should be conducted to derive rates and coefficients where literature values cannot be obtained or where they are found to be inadequate for oil sands pit lakes. This may be done on single variables or on groups of processes, depending on the availability of data. For example, laboratory-scale tests may be used to determine the values of single variables, which can then be tested in the model. Data that might be obtained in field studies, which were not available at the time of model development but might be significant drivers, are listed below:

    a. concentrations of nutrients and carbon forms in MFT porewater
    b. temperature, pH and other physiochemical characteristics of MFT porewater
    c. size and composition of bubbles formed by methanogenesis
    d. physical characteristics and variability of cracks formed by long-term bubble formation
    e. influence of the FFT layer on released porewater

    Other data may be more appropriately collected by laboratory studies. Such data may include the following:

    a. kinetic rates of diagenetic reactions
    b. inhibition (or stimulation) of methanogenesis due to the presence of nitrogen and sulphur compounds

Depending on the desired rate of progress, some of these steps could be completed concurrently and by multiple organizations. In any case, most or all of these four steps will need to be completed to ensure the model is validated, defensible and set up appropriately, prior to attempting to use it for predictive simulations.

4.0 REFERENCES

Algar, C.K. and B.P. Boudreau. 2009. Transient growth of an isolated bubble in muddy, fine-grained sediments. Geochimica et Cosmochimica Acta. 73(9):2581-2591.

Antenucci, J. and A. Imerito. 2002. The CWR Dynamic Reservoir Simulation Model DYRESM: Science Manual. Center for Water Research 44 pp.

Bédard, C. and R. Knowles. 1989. Physiology, Biochemistry, and Specific Inhibitors of CH_4, NH_4^+ and CO Oxidation by Methanotrophs and Nitrifiers. Microbiological Reviews. 53:68-84.

Bédard, C. and R. Knowles. 1997. Some properties of methane oxidation in a thermally stratified lake. Canadian Journal of Fisheries and Aquatic Sciences. 54: 1639–1645.

Boeckx, P. and O. van Cleemput. 1996. Methane Oxidation in a Neutral Landfill Cover Soil: Influence of Moisture Content, Temperature, and Nitrogen-Turnover. Journal of Environmental Quality. 25(1):178-183.

Boudreau, B.P. 1997. Diagenetic models and their implementation. Springer Verlag. Berlin. 414 p.

Boudreau, B.P., B.S. Gardiner and B.D. Johnson. 2001a. Rate of growth of isolated bubbles in sediments with a diagenetic source of methane. Limnol. Oceanogr. 46(3): 616–622.

Boudreau, B.P., B.S. Gardiner and B.D. Johnson. 2001b. Errata to Rate of growth of isolated bubbles in sediments with a diagenetic source of methane. Limnol. Oceanogr. 46(6):1578.

Boudreau, B.P., C. Algar, B.D. Johnson, I. Croudace, A. Reed, Y. Furukawa, K.M. Dorgan, P.A. Jumars, A.S. Grader and B.S. Gardiner. 2005. Bubble growth and rise in soft sediments. Geology. 33(6):517–520.

Brennen, C.E. 1995. Cavitation and bubble dynamics. Oxford University Press, New York. 293pp.

Cai, Z. and X. Yan. 1999. Kinetic Model by Methane Oxidation by Paddy Field as Affected by Temperature, Moisture and N Addition. Soil Biology and Biochemistry. 31:715-725.

CEMA (Cumulative Environmental Management Association). 2006. Modelling Assessment of End Pit Lakes Meromictic Potential. Prepared by Golder Associates Ltd. for CEMA. Available at http://www.cemaonline.ca/index.php/working-groups/reclamation-working-group-(rwg).

CEMA. 2007. Pit Lake Modelling Phase II. Prepared by Golder Associates Ltd. for CEMA. Available at http://www.cemaonline.ca/index.php/working-groups/reclamation-working-group-(rwg).

Cole, T.M. and S.A. Wells. 2001. CE-QUAL-W2: A Two-Dimensional, Laterally Averaged, Hydrodynamic and Water Quality Model, Version 3.1. Prepared for U.S. Army Corps of Engineers, Washington, DC 20314-1000.

Cole, T.M. and S.A. Wells. 2008. CE-QUAL-W2: A Two-Dimensional, Laterally Averaged, Hydrodynamic and Water Quality Model, Version 3.6. Prepared for U.S. Army Corps of Engineers, Washington, DC 20314-1000.

DiToro, D.M. 2001. Sediment Flux Modeling. Wiley-Interscience. New York. 656pp.

Dumestre, J.F., J. Guezennec, C. Galy-Lacaux, R. Delmas, S. Richard and L. Labroue. 1999. Influence of light intensity on methanotrophic bacterial activity in Petit-Saut reservoir, French Guiana. Applied and Environmental Microbiology. 65: 534– 539.

Eckert, W.F., J.H. Masliyah, M.R. Gray and P.M. Fedorak. 1996. Prediction of sedimentation and consolidation of fine tails. AIChE Journal. 42(4):960-972.

Fedorak, P.M., D.L. Coy, M.J. Salloum and M.J. Dudas. 2002. Methanogenic potential of tailings samples from oil sands extraction plants. Canadian Journal of Microbiology. 48:21-33.

Fedorak, P.M., D.L. Coy, M.J. Dudas, M.J. Simpson, A.J. Renneberg and M.D. MacKinnon. 2003. Microbially-mediated fugative gas production from oil sands tailings and increased tailings densification rates. Journal of Environmental Engineering and Science. 2:199-211.

Foght, J.M., P.M. Fedorak and D.W.S. Westlake. 1985. Microbial content and metabolic activities in Syncrude tailings pond. AOSTRA Journal of Research. 1:139-146.

Foght, J.M., D. Bressler, M. Cardenas, P.M. Fedorak, S. Guigard, R. Gupta and T. Siddique. 2010. Microbial activity influences pore water recovery from oil sands mature fine tailings. CONRAD Water Usage Workshop and Seminar. April 22, 2010. Edmonton, AB.

Gardiner, B.S., B.P. Boudreau and B.D. Johnson. 2003. Growth of disk-shaped bubbles in sediments. Geochimica et Cosmochimica Acta. 67:1485-1494.

Guerin, F. and G. Abril. 2007. Significance of pelagic aerobic methane oxidation in the methane and carbon budget of a tropical reservoir. Journal of Geophysical Research. 112: G03006, doi:10.1029/2006JG000393.

Harrits, S.M. and R.S. Hanson. 1980. Stratification of aerobic methane-oxidizing organisms in Lake Mendota, Madison, Wisconsin. Limnology and Oceanography. 25(3):412-421.

Haveroen, M.E., M.D. MacKinnon and P.M. Fedorak. 2005. Polyacrylamide added as a nitrogen source stimulates methanogenesis in consortia from various wastewaters. Water Research. 39(14): 3333-3341.

Holowenko, F.M. 2000. Methanogenesis and fine tailings waste from oil sands extraction: a microcosm-based laboratory examination. M.Sc. Thesis. University of Alberta. Edmonton, Ab. 203pp.

Holowenko, F.M., M.D. MacKinnon and P.M. Fedorak. 2000. Methanogens and sulfate-reducing bacteria in oil sands fine tailings waste. Canadian Journal of Microbiology. 46(10):927-937.

Holowenko, F.M., M.D. MacKinnon and P.M. Fedorak. 2001. Naphthenic acids and surrogate naphthenic acids in methanogenic microcosms. Water Research. 35:2595-2606.

Hosokawa, S. and A. Tomiyama. 2010. Effects of Bubbles on Turbulent Flows in Vertical Channels. 7th International Conference on Multiphase Flow. ICMF 2010, May 30-June 4, 2010, Tampa, FL.

Hwang, K.N, and A.J. Mehta, 1989: Fine sediment erodibility in Lake Okeechobee. Coastal and Oceanographic Engineering Dept., University of Florida, Report UFL/COEL-89/019, Gainsville, FL.

Johnson, B.D., B.P. Boudreau, B.S. Gardiner and R. Maass. 2002. Mechanical response of sediments to bubble growth. Marine Geology. 187:347-363.

Jones, C. and W. Lick. 1999. “Effects of Bed Coarsening on Sediment Transport”. Estuarine and Coastal Modeling. *Proceedings of the sixth international conference*. Pp 915 – 930.

Jones, R.D. and R.Y. Morita. 1983. Methane oxidation by *Nitrosococcus oceanus* and *Nitrosomonas europaea*. Appl. Environ Microbiol. 45(2):401-410.

Kelley, C. 2003. Methane oxidation potential in the water column of two diverse coastal marine sites. Biogeochemistry. 65: 105–120.

King, I.P. 1985. Strategies of Finite Element Modeling of Three-dimensional Hydrodynamic Systems. In Advances in Water Resources, 8:69-76.

King, G.M. and S. Schnell. 1994. Effect of Increasing Atmospheric Methane Concentration on Ammonium Inhibition of Soil Methane Consumption. Nature. 307(6487):282-284.

Klein, S. 2006. Sediment porewater exchange and solute release during ebullition. Maritime Chemistry. 102:60-71.

Lidstrom, M.E. and L. Somers. 1984. Seasonal study of methane oxidation in Lake Washington. Applied & Environmental Microbiology. 47(6):1255-1260.

Liikanen, A., J.T. Huttunen, K. Valli, and P.J. Martikainen. 2002. Methane cycling in the sediment and water column of mid-boreal hypereutrphic Lake Kevaton, Finland. Arch. Hydrobiol.154: 585–603.

Martens C.S. and J.V. Klump. 1980. Biogeochemical cycling in an organic-rich coastal marine basin-I. Methane sediment-water exchange processes. Geochim. Cosmochim. Acta. 44:471-490.

Mikula, R.J., K.L. Kasperski, R.D. Burns and M.D. MacKinnon. 1996. Nature and Fate of Oil Sands Fine Tailings. In *Schramm, L.L., Suspensions: Fundamentals and Applications in the Petroleum Industry*. American Chemical Society.

Packman, J.J., K.J., Comings, and D.B. Booth. 1999. Using turbidity to determine total suspended solids in urbanizing streams in the Puget Lowlands: in Confronting Uncertainty: Managing Change in Water Resources and the Environment, Canadian Water Resources Association annual meeting, Vancouver, BC, 27–29 October 1999, p. 158–165.

Rudd, J.W.M., A. Furutani, R.J. Flett and R.D. Hamilton. 1976. Factors controlling methane oxidation in shield lakes: the role of nitrogen fixation and oxygen concentration. Limnology and Oceanography. 21(3):357-364.

Rudd, J.W.M., R.D. Hamilton and N.E.R. Campbell. 1974. Measurements of microbial oxidation of methane in lake water. Limnology and Oceanography. 19: 519– 524.

Schmidt, U. and Conrad, R. 1993. Hydrogen, carbon monoxide and methane dynamics in lake constance. Limnology and Oceanography. 38: 1214–1226.

Shell (Shell Canada Limited). 2007. Jackpine Mine Expansion & Pierre River Mine Project Application and Environmental Impact Assessment. Volumes 1, 2, 3, 4 and 5. Submitted to Alberta Energy and Utilities Board and Alberta Environment, December 2007. Calgary, AB.

Shell. 2009. Shell Albian Sands Muskeg River Mine Expansion Draft No Net Loss Lake Plan. Submitted to Fisheries and Oceans Canada July 31, 2009. Calgary, AB.

Siddique, T., P.M. Fedorak and J.M. Foght. 2006. Biodegradation of short-chain n-alkanes in oil sands tailing under methanogenic conditions. Environmental Science & Technology. 40:5459-5464.

Siddique, T., P.M. Fedorak, M.D. MacKinnon and J.M. Foght. 2007. Metabolism of BTEX and naphtha compounds to methane in oil sands tailings. Environmental Science & Technology. 41:2350-2356.

Siddique, T., R. Gupta, P.M. Fedorak, M.D. MacKinnon and J.M. Foght. 2008. A first approximation model to predict methane generation from an oil sands tailings settling Basin. Chemosphere. 72:1573-1580.

Sobolewski, A. 1992. The microbial characteristics of oil sands tailings sludge. Consultant's report submitted to AOSTRA. Calgary, Ab.

Striegl, R.G., and Michmerhuizen, C.M., 1998. Hydrologic influence on methane and carbon dioxide dynamics at two north-central Minnesota lakes. Limnology and Oceanography. 43: 1519– 1529.

Suthaker, N.N. 1995. Geotechnics of oil sand fine tailings. Ph.D. Thesis. University of Alberta, Edmonton, AB.

Tetra Tech (Tetra Tech Inc.). 2002: Theoretical and computational aspects of sediment and contaminant transport in EFDC. A report to the U.S. Environmental Protection Agency, Fairfax, VA.

Umorin, P.P. 2002. Mathematical modelling of the effect of protozoa on methane bacterial oxidation in water bodies. Water Resources. 29(2):196-201.

Utsumi, M., Y. Nojiri, T. Nakamura, T. Nozawa, A. Otsuki, N. Takamura, M. Watanabe and H. Seki. 1998a. Dynamics of dissolved methane and methane oxidation in dimictic Lake Nojiri during winter. Limnology and Oceanography. 43: 10–17.

Utsumi, M., Y. Nojiri, T. Nakamura, T. Nozawa, A. Otsuki and H. Seki. 1998b. Oxidation of dissolved methane in a eutrophic, shallow lake: Lake Kassumigaura, Japan. Limnology and Oceanography. 43: 471–480.

van Kesteren, W. and T. van Kessel. 2002a. Gas bubble nucleation and growth in cohesive sediments. In: JC Winterwerp and C Kranenburg, Editors, Fine Sediment Dynamics in the Marine Environment. Proc Marine Science 5, Elsevier, Amsterdam. pp. 329–341.

van Kesteren, W. and T. van Kessel. 2002b. Gas production and transport in artificial sludge depots. Waste Management. 22:19-28.

van Rijn, L.C. 1984. Sediment Transport, Part II: Suspended Load Transport. Journal of Hydraulic Engineering, ASCE, Vol 110, No 11. pp. 1613-1641

Venkiteswarran, J. J. and S.L. Schiff. 2005. Methane oxidation: isotopic enrichment factors in freshwater boreal reservoirs. Applied Geochemistry. 20: 683– 690.

Ward, B.B. and K.A. Kilpatrick. 1990. Relationship between substrate concentration and oxidation of ammonium and methane in a stratified water column. Continental Shelf Res. 10: 1193–1208.

Wheeler, S. J. 1988. A conceptual model for soils containing large gas bubbles. Geotech. **38:** 389–397.

Yuan, Q.Z., K.T. Valsaraj, D.D. Reible and C.S. Willson. 2007. A laboratory study of sediment and contaminant release during gas ebullition. J. Air Waste Manage. Assoc. 57:1103-1111.

Yuan, Q.Z., K.T. Valsaraj and D.D. Reible. 2009. A model for contaminant and sediment transport via gas ebullition through a sediment cap. Environmental Engineering Science. 26(9):1381-1931.

Zheng, L. and P.D. Yapa. 2000. Buoyant velocity of spherical and non-spherical bubbles/ droplets. Journal of Hydraulic Engineering, ASCE, November, 852-855.

Report Signature Page

PREPARED BY

Shwet Prakash, M.S.
Project Manager, Surfacewater Modeling Group
ERM Inc.

Jerry Vandenberg, M.Sc.
Associate, Senior Water Quality Specialist
Golder Associates Ltd.

REVIEWED BY

Edward Buchak, P.H.
Partner and Manager, Surfacewater Modeling Group
ERM Inc.

\\cal1-s-filesrv1.golder.gds\data\active_2009\1336\09-1336-1008 - cema pit lake model\reporting\draft 2 may 2011\cema oil sands pit lake model may 2011.docx

APPENDIX A

Input Data Description

APPENDIX A
Input Data Description

This appendix describes the input files necessary to run the OSPLM. The descriptions follow the format of the CE-QUAL-W2 v.3.6 manual, Appendix C (Cole and Wells 2008).

There is one essential input files "W2_CEMA_Input.npt" that includes the model setup for the entire CEMA related modeling. The following description provides information on this file.

Consolidation rates for different consolidation regions can be provided to the model in the form of a time varying input files. Description of this file is provided at the end of this appendix.

Typically each line in "W2_CEMA_Input.npt" has two fields, input data description and the input data (see example below), separated by a comma.

Example 1:

Input data description, Input data

"Switch to perform bed consolidation,", .TRUE.

Exception to this rule is when input data are defined for multiple regions or periods. In such cases the number of fields for "Input Data" corresponds to the number of regions/periods (see example below):

Example 1:

Input data description, Input data

"FFT Layer Number of Periods,", 3

Input data description, Input data for Period 1, Input data for Period 2, Input data for Period 3

"FFT Layer Start Times,", 1,100,200

"FFT Layer End Times,", 50,150,350

Example 2:

Input data description, Input data

"Number of regions for different initial sediment concentrations,", 2

Input data description, Input data for Region 1, Input data for Region 2

"Starting segment for regions,", 2, 6

"Ending segment for regions,", 5, 11

Bed Consolidation

Field	Name	Value	Default	Description
1	IncludeBedConsolidation	Logical	True	Switch to perform bed consolidation
2	LayerAddThkFrac	Real	1.0	Fraction of layer thickness at which water layer is added
3	NumConsolidRegns	Integer		Number of bed consolidation regions
4	ConsRegSegSt	Integer		Starting segment for regions
5	ConsRegSegEn	Integer		Ending segment for regions
6	ConsolidationType	Integer		Data type for bed consolidation for each region
7	ConstConsolidRate	Real		Bed consolidation rate (m/d)
8	ConsolidRateRegnFil	Character		Bed consolidation data file

Example

"Switch to perform bed consolidation,", .TRUE.

"Fraction of layer thickness at which water layer is added,", 1.0

"Number of bed consolidation regions,", 1

"Starting segment for regions,", 2

"Ending segment for regions,", 11

"Data type for bed consolidation for each region (0: Constant, 1: Time varying),", 1

"Bed consolidation rate (m/d),", 0.02739726

"Bed consolidation data file,", "Regn1.npt,"

Initial Conditions

Field	Name	Value	Default	Description
1	BedElevationInit	Real		Initial bed elevation (m)
2	BedPorosityInit	Real		Initial sediment bed porosity
3	CEMAPWTemperature	Real		Porewater Temperature (C)
4	CEMAPWpH	Real		Porewater pH

Example

"Initial bed elevation in meters,", 10

"Initial sediment bed porosity,", 0.8

"Porewater Temperature (C),", 20.0

"Porewater pH,", 8.5

Sediment Characteristics

Field	Name	Value	Default	Description
1	CEMAParticleSize	Real	1000.0	Sediment bed particle size (microns)
2	CEMASedimentType	Integer		Sediment type 1: Cohesive, 2: Non-cohesive
3	CEMASedimentDensity	Real	2600	Sediment bulk density (kg/m³)
4	CEMASedimentSVelocity	Real	5.0	Sediment particle settling velocity (m/d)
5	CEMASedimentProcessesInc	Logical	True	Switch to include sediment resuspension and deposition processes

Example

"Sediment bed particle size in microns,", 100

"Sediment type 1: Cohesive, 2: Non-cohesive,", 2

"Sediment bulk density (kg/m³),", 2600

"Sediment particle settling velocity (m/d),", 5.0

"Include sediment resuspension and deposition processes,", .TRUE.

Consolidation Output

Field	Name	Value	Default	Description
1	WriteBESnp	Logical	True	Switch to write bed elevation snapshot output
2	WritePWSnp	Logical	True	Switch to write bed porosity snapshot output

Example

"Write bed elevation snapshot output,", .TRUE.

"Write bed porosity snapshot output,", .TRUE.

FFT Layer

Field	Name	Value	Default	Description
1	IncludeFFTLayer	Logical	True	Switch to include FFT Layer
2	NumFFTActivePrds	Integer		FFT Layer Number of Periods
3	FFTActPrdSt	Real		FFT Layer Start Times
4	FFTActPrdEn	Real		FFT Layer End Times
5	InitFFTLayerConc	Real	360000	Initial tailings concentration in FFT (gm/m^3)
6	FFTLayerSettVel	Real		Settling velocity of FFT to MFT (m/d)
7	MoveFFTLayerDown	Logical	True	Switch to move FFT layer during consolidation

Example

"Include FFT Layer,", .TRUE.

"FFT Layer Number of Periods,", 3

"FFT Layer Start Times,", 1,100,200

"FFT Layer End Times,", 50,150,350

"Initial tailings concentration in FFT (gm/m^3),", 360000

"Settling velocity of FFT to MFT (m/d),", 0.d0

"Move FFT layer during consolidation,", .TRUE.

Diagenesis Initial Conditions

Field	Name	Value	Default	Description
1	IncludeCEMASedDiagenesis	Logical	True	Switch to include sediment diagenesis processes
2	NumRegnsSedimentBedComposition	Integer		Number of regions for different initial sediment concentrations
3	SedBedInitRegSegSt	Integer		Starting segment for regions
4	SedBedInitRegSegEn	Integer		Ending segment for regions
5	SDRegnPOC_T	Real		Initial particulate organic carbon (total) concentration for each region (mgC/l)
6	SDRegnPON_T	Real		Initial particulate organic nitrogen (total) concentration for each region (mgN/l)
7	SDRegnSul_T	Real		Initial sulfate concentration for each region (mg-S/l)
8	SDRegnNH3_T	Real		Initial dissolved ammonia concentration for each region (mg-N/l)
9	SDRegnH2S_T	Real		Initial dissolved sulfide concentration for each region (mg-S/l)
10	SDRegnCH4_T	Real		Initial dissolved methane concentration for each region (mg-C/l)

Example

"Include sediment diagenesis processes,", .TRUE.

"Number of regions for different initial sediment concentrations,", 2

"Starting segment for regions,", 2, 6

"Ending segment for regions,", 5, 11

"Initial particulate organic carbon (total) concentration for each region mgC/l,", 70, 80

"Initial particulate organic nitrogen (total) concentration for each region mgN/l,", 100, 80

"Initial sulfate concentration for each region mg-S/l,", 1.5, 10.0

"Initial dissolved ammonia concentration for each region mgN/l,", 0.10, 0.11

"Initial dissolved sulfide concentration for each region mgS/l,", 0.15, 0.14

"Initial dissolved methane concentration for each region mgC/l,", 0.12, 0.13

Generic BOD constituent Settings

Field	Name	Value	Default	Description
1	IncludeCEMAGenBODConstituents	Logical	True	Switch to include generic BOD constituents in sediments
2	NumGenBODConstituents	Integer		Number of generic BOD constituents
3	SedGenBODName	String		Generic BOD constituent names
4	NumGenBODInitRegns	Integer		Number of regions for different initial generic BOD concentrations
5	SedGenBODRegSegSt	Integer		Starting segment for regions
6	SedGenBODRegSegEn	Integer		Ending segment for regions
7	SedGenBODInit	Real		Initial generic BOD concentration for each region (mg/l)

Example

"Include generic sediment BOD constituents,", .TRUE.

"Number of generic sediment BOD constituents,", 3

"Generic sediment BOD constituent names,","SBOD1","SBOD2","SBOD3"

"Number of regions for initializing generic sediment BOD constituents,", 2

"Starting segment for generic BOD initialization for each region,", 2, 5

"Ending segment for generic BOD initialization for each region,", 4, 7

"Initial concentration for generic BOD per region mg/l,",0.65, 0.75

"Initial concentration for generic BOD per region mg/l,",0.75, 0.85

"Initial concentration for generic BOD per region mg/l,",0.85, 0.65

Generic BOD rate Settings

Field	Name	Value	Default	Description
1	NumGenBODConsumptionRegions	Integer		Number of regions for different generic BOD consumption rates
2	SedGenBODConsRegSegSt	Integer		Starting segment for regions
3	SedGenBODConsRegSegEn	Integer		Ending segment for regions
4	SedGenBODRegnRate	Real		Generic BOD consumption rate for each region
5	SedGenBODRegnTCoeff	Real		Generic BOD temperature coefficient for each region

Example

"Number of regions for different generic sediment BOD constituent consumption rate,", 2

"Starting segment for generic BOD consumption for each region,", 2, 5

"Ending segment for generic BOD consumption for each region,", 4, 7

"Consumption rate for generic BOD per region 1/d,",0.065, 0.065

"Consumption rate for generic BOD per region 1/d,",0.065, 0.065

"Consumption rate for generic BOD per region 1/d,",0.065, 0.065

"Temperature coefficient for generic BOD decay per region,",1.01, 1.01

"Temperature coefficient for generic BOD decay per region,",1.02, 1.02

"Temperature coefficient for generic BOD decay per region,",1.03, 1.03

Diagenesis Region Settings

Field	Name	Value	Default	Description
1	NumRegnsSedimentDiagenesis	Integer		Number of regions for different diagenesis related rates
2	SedBedDiaRCRegSegSt	Integer		Starting segment for regions
3	SedBedDiaRCRegSegEn	Integer		Ending segment for regions
4	SDRegnPOC_L_Fr	Real		Fraction of labile POC for each diagenesis region
5	SDRegnPOC_R_Fr	Real		Fraction of refractory POC for each diagenesis region
6	SDRegnPON_L_Fr	Real		Fraction of labile PON for each diagenesis region
7	SDRegnPON_R_Fr	Real		Fraction of refractory PON for each diagenesis region

Example

"Number of regions for different diagenesis related rates,", 2

"Starting segment for regions,", 2, 6

"Ending segment for regions,", 5, 11

"Fraction of labile poc for each diagenesis region,",0.65, 0.65

"Fraction of refractory poc for each diagenesis region,",0.25, 0.25

"Fraction of labile pon for each diagenesis region,",0.65, 0.65

"Fraction of refractory pon for each diagenesis region,",0.2, 0.2

Diagenesis Rates Settings Part 1

Field	Name	Value	Default	Description
1	SDRegnPW_DiffCoeff	Real	0.001	Porewater diffusion coefficient (m^2/d)
2	SDRegnOx_Threshold	Real	2.0	DO Threshold for aerobic layer oxidation rates (mgO2/l)
3	SDRegnAe_NH3_NO3_L	Real	0.131	Nitrification rate in aerobic layer (NH_3->NO_3) at DO below threshold (m/d)
4	SDRegnAe_NH3_NO3_H	Real	0.131	Nitrification rate in aerobic layer (NH_3->NO_3) at DO above threshold (m/d)
5	SDRegnAe_NO3_N2_L	Real	0.100	Denitrification rate in aerobic layer (NO_3->N_2) at DO below threshold (m/d)
6	SDRegnAe_NO3_N2_H	Real	0.100	Denitrification rate in aerobic layer (NO_3->N_2) at DO above threshold (m/d)
7	SDRegnAn_NO3_N2	Real	0.100	Denitrification rate in anerobic layer (NO_3->N_2) (m/d)
8	SDRegnAe_CH4_CO2	Real	0.700	Methane oxidation rate in aerobic layer (m/d)
9	SDRegnAe_HS_NH4_Nit	Real	0.728	Nitrification half-saturation constant for NH_4N in aerobic layer (mgN/l)
10	SDRegnAe_HS_O2_Nit	Real	0.370	Nitrification half-saturation constant for O_2 in aerobic layer (mgO_2/l)

Example

"Porewater diffusion coefficient m²/d,",0.001,0.001

"DO Threshold for aerobic layer oxidation rates mgO2/l,",2.0,2.0

"Nitrification rate in aerobic layer (NH3->NO3) at DO below threshold m/d,",0.131, 0.131

"Nitrification rate in aerobic layer (NH3->NO3) at DO above threshold m/d,",0.131, 0.131

"Denitrification rate in aerobic layer (NO3->N2) at DO below threshold m/d,",0.1 ,0.1

"Denitrification rate in aerobic layer (NO3->N2) at DO above threshold m/d,",0.1 ,0.1

"Denitrification rate in anerobic layer (NO3->N2) m/d,",0.1 ,0.1

"Methane oxidation rate in aerobic layer m/d,",0.7, 0.7

"Nitrification half-saturation constant for NH4N in aerobic layer mgN/l,",0.728,0.728

"Nitrification half-saturation constant for O2 in aerobic layer mgO2/l,",0.37,0.37

Diagenesis Rates Settings Part 2

Field	Name	Value	Default	Description
1	SDRegn_Theta_PW	Real	1.08	Temperature coefficient for porewater diffusion between layers
2	SDRegn_Theta_NH3_NO3	Real	1.08	Temperature coefficient for nitrification
3	SDRegn_Theta_NO3_N2	Real	1.08	Temperature coefficient for denitrification
4	SDRegn_Theta_CH4_CO2	Real	1.08	Temperature coefficient for methane oxidation
5	SDRegn_Sulfate_CH4_H2S	Real	20.0	Sulfate concentration above which sulfide over methane is produced (mgS/l)
6	SDRegnAe_H2S_SO4	Real	0.200	Sulfide oxidation rate in aerobic layer m/d
7	SDRegn_Theta_H2S_SO4	Real	1.08	Temperature coefficient for sulfide oxidation
8	SDRegn_NormConst_H2S_SO4	Real	4.0	Sulfide oxidation normalization constant for O_2 (mgO_2/l)
9	SDRegn_MinRate_PON_Lab	Real	0.035	Mineralization rate for labile PON (1/d)
10	SDRegn_MinRate_PON_Ref	Real	0.0018	Mineralization rate for refractory PON (1/d)

Example

"Temperature coefficient for porewater diffusion between layers,",1.08, 1.08

"Temperature coefficient for nitrification,",1.123, 1.123

"Temperature coefficient for denitrification,",1.08, 1.08

"Temperature coefficient for methane oxidation,",1.079, 1.079

"Sulfate concentration above which sulfide over methane is produced mgS/l,",20.0, 2.0

"Sulfide oxidation rate in aerobic layer m/d,",0.2, 0.2

"Temperature coefficient for sulfide oxidation,",1.08, 1.08

"Sulfide oxidation normalization constant for O2 mgO2/l,",4.0, 4.0

"Mineralization rate for labile PON 1/d,",0.035, 0.035

"Mineralization rate for refractory PON 1/d,",0.0018, 0.0018

Diagenesis Rates Settings Part 3

Field	Name	Value	Default	Description
1	SDRegn_MinRate_PON_Ine	Real	0.0	Mineralization rate for inert/slow refractory PON (1/d)
2	SDRegn_MinRate_POC_Lab	Real	0.035	Mineralization rate for labile POC (1/d)
3	SDRegn_MinRate_POC_Ref	Real	0.0018	Mineralization rate for refractory POC (1/d)
4	SDRegn_MinRate_POC_Ine	Real	0.0	Mineralization rate for inert/slow refractory POC (1/d)
5	SDRegn_Theta_PON_Lab	Real	1.08	Temperature coefficient for labile PON
6	SDRegn_Theta_PON_Ref	Real	1.08	Temperature coefficient refractory PON
7	SDRegn_Theta_PON_Ine	Real	1.08	Temperature coefficient inert/slow refractory PON
8	SDRegn_Theta_POC_Lab	Real	1.08	Temperature coefficient labile POC
9	SDRegn_Theta_POC_Ref	Real	1.08	Temperature coefficient refractory POC
10	SDRegn_Theta_POC_Ine	Real	1.08	Temperature coefficient for inert/slow refractory POC

Example

"Mineralization rate for inert/slow refractory PON 1/d,",0.0, 0.0

"Mineralization rate for labile POC 1/d,",0.035, 0.035

"Mineralization rate for refractory POC 1/d,",0.0018, 0.0018

"Mineralization rate for inert/slow refractory POC 1/d,",0.0, 0.0

"Temperature coefficient for labile PON,",1.1, 1.1

"Temperature coefficient refractory PON,",1.15, 1.15

"Temperature coefficient inert/slow refractory PON,",1.17, 1.17

"Temperature coefficient labile POC,",1.1, 1.1

"Temperature coefficient refractory POC,",1.15, 1.15

"Temperature coefficient for inert/slow refractory POC,",1.17, 1.17

Methane Calculation Setting

Field	Name	Value	Default	Description
1	SDRegn_CH4CompMethod	Integer	0	Methane production calculation method (0: Analytical, 1: Numerical)

Example

"Methane production calculation method (0: Analytical, 1: Numerical),", 0, 0

Ionization Settings

Field	Name	Value	Default	Description
1	NH4_NH3_Eqb_Const	Real	9.1	Equilibrium constant for NH4+ <-> NH3 ionization. Provide as pK
2	HS_H2S_Eqb_Const	Real	9.0	Equilibrium constant for HS- <-> H2S ionization. Provide as pK

Example

"Equilibrium constant for NH4+ <-> NH3 ionization. Provide as pK,", 9.1

"Equilibrium constant for HS- <-> H2S ionization. Provide as pK,", 9.0

Dissolution Settings

Field	Name	Value	Default	Description
1	HenryConst_NH3	Real	0.0179	Henry's constant for NH_3d <-> NH_3g (atm/M)
2	HenryConst_CH4	Real	469.0	Henry's constant for CH_4d <-> CH_4g (atm/M)
3	HenryConst_H2S	Real	10.0	Henry's constant for H_2Sd <-> H_2Sg (atm/M)
4	HenryConst_CO2	Real	29.0	Henry's constant for CO_2d <-> CO_2g (atm/M)

Example

"Henry's constant for NH3d <-> NH3g in atm/M,", 0.0179

"Henry's constant for CH4d <-> CH4g in atm/M,", 469

"Henry's constant for H2Sd <-> H2Sg in atm/M,", 10

"Henry's constant for CO2d <-> CO2g in atm/M,", 29

Gas Bubble Formation Rates

Field	Name	Value	Default	Description
1	GasDiff_Sed	Real	$1X10^{-9}$	Gas diffusion coefficient in sediment (m^2/s)
2	CalibParam_R1	Real	0.0014	Calibration parameter R1 (m)
3	YoungModulus	Real	$1.4X10^{9}$	Young's modulus E (N/m^2)
4	CritStressIF	Real	300.0	Critical stress intensity factor for sediments K1c (N/m^3/2)
5	BubbRelScale	Real	0.02	Bubbles release scale
6	CrackCloseFraction	Real	0.20	Fraction of critical pressure at which cracks close
7	LimBubbSize	Logical	True	Switch to limit bubble size
8	MaxBubbRad	Real	80.0	Maximum bubble radius (mm)
9	UseReleaseFraction	Logical	True	Switch to use slow release of bubbles
10	BubbRelFraction	Real	0.005	Bubbles release fraction (sediments)
11	BubbAccFraction	Real	0.10	Bubbles accumulation fraction
12	NumBubRelArr	Integer	2000	Number of bubbles release array
13	BubbRelFractionAtm	Real	0.001	Bubbles release fraction (atmosphere)
14	BubbWatGasExchRate	Real	$1X10^{-7}$	Bubbles-Water gas exchange rate (1/s)

Example

"Gas diffusion coefficient in sediment in m²/s,", 1.0d-9
"Calibration parameter R1 in m,", 0.0014
"Young's modulus E in N/m²,", 1.4d+9
"Critical stress intensity factor for sediments K1c in N/m^3/2,", 300
"Bubbles release scale,", 0.02
"Fraction of critical pressure at which cracks close,", 0.20
"Switch to limit bubble size,", .TRUE.
"Maximum bubble radius in mm,", 80
"Switch to use slow release of bubbles,", .TRUE.
"Bubbles release fraction (sediments),", 0.005
"Bubbles accumulation fraction,", 0.1
"Number of bubbles release array,", 2000
"Bubbles release fraction (atmosphere),", 0.001
"Bubbles-Water gas exchange rate (1/s),",1.0d-7

Bubbles Related Turbulence

Field	Name	Value	Default	Description
1	ApplyBubbTurb	Logical	True	Apply additional turbulence due to bubbles release
2	CEMATurbulenceScaling	Real	0.0001	Scaling factor for bubbles related turbulence

Example

"Apply additional turbulence due to bubbles release,",.TRUE.

"Turbulence scaling factor for bubbles release,",0.0001

Turbidity Calculations

Field	Name	Value	Default	Description
1	CoeffA_Turb	Real	1.243	Coefficient Aturb in Aturb*ln(TSS) + Bturb = ln(Turbidity)
2	CoeffB_Turb	Real	-0.294	Coefficient Bturb in Aturb*ln(TSS) + Bturb = ln(Turbidity)

Example

"Coefficient Aturb in Aturb*ln(TSS) + Bturb = ln(Turbidity),",1.243

"Coefficient Bturb in Aturb*ln(TSS) + Bturb = ln(Turbidity),",-0.294

Sediment Flux Output Settings

Field	Name	Value	Default	Description
1	WriteCEMAMFTSedFlx	Logical	True	Switch to write sediment fluxes

Example

"Write sediment fluxes,", .TRUE.

External Time Varying File for Consolidation Rate

Column	Name	Value	Description
1	JDAY	Real	Julian Days
2	Consolidation Rate	Real	Consolidation Rate in m/d

Example

$Bed consolidation (m/d) rate

JDay Consolidation

1.000 0.02740

2.000 0.02740

3.000 0.02740

4.000 0.02740

5.000 0.02740

6.000 0.02740

\\cal1-s-filesrv1.golder.gds\data\active_2009\1336\09-1336-1008 - cema pit lake model\reporting\draft 2 may 2011\app a input data.doc

APPENDIX B

Sample Input Files

W2_CEMA_INPUT.NPT

$Additional CEMA related W2 input

$Please see help file for input description

$All lines starting with $ are comments and disregarded by the model

"Switch to perform bed consolidation,", .TRUE.

"Fraction of layer thickness at which water layer is added,", 1.0

"Number of bed consolidation regions,", 1

"Starting segment for regions,", 2

"Ending segment for regions,", 7

"Data type for bed consolidation for each region (0: Constant, 1: Time varying),", 1

"Bed consolidation rate (m/d),", 0.02739726

"Bed consolidation data file,", "Regn1.npt,"

"Initial bed elevation in meters,", 10

"Initial sediment bed porosity,", 0.8

"Porewater Temperature (C),", 20.0

"Porewater pH,", 8.5

"Sediment bed particle size in microns,", 100

"Sediment type 1: Cohesive, 2: Non-cohesive,", 2

"Sediment bulk density (kg/m^3),", 2600

"Sediment particle settling velocity (m/d),", 5.0

"Include sediment resuspension and deposition processes,", .TRUE.

"Write bed elevation snapshot output,", .TRUE.

"Write bed porosity snapshot output,", .TRUE.

"Include FFT Layer,", .TRUE.

"FFT Layer Number of Periods,", 5

"FFT Layer Start Times,", 1,65,125,200,300

"FFT Layer End Times,", 50,100,175,250,400

"Initial tailings concentration in FFT (gm/m^3),", 360000

"Settling velocity of FFT to MFT (m/d),", 0.d0

"Move FFT layer during consolidation,", .TRUE.

"Include sediment diagenesis processes,", .TRUE.

"Number of regions for different initial sediment concentrations,", 2

"Starting segment for regions,", 2, 5

"Ending segment for regions,", 4, 7

"Initial particulate organic carbon (total) concentration for each region mgC/l,", 70, 80

"Initial particulate organic nitrogen (total) concentration for each region mgN/l,", 100, 80

"Initial sulfate concentration for each region mgS/l,", 1.5, 10.0

"Initial dissolved ammonia concentration for each region mgN/l,", 0.10, 0.11

"Initial dissolved sulfide concentration for each region mgS/l,", 0.15, 0.14

"Initial dissolved methane concentration for each region mgC/l,", 0.12, 0.13

"Include generic sediment BOD constituents,", .TRUE.

"Number of generic sediment BOD constituents,", 3

"Generic sediment BOD constituent names,","SBOD1","SBOD2","SBOD3"

"Number of regions for initializing generic sediment BOD constituents,", 2

"Starting segment for generic BOD initialization for each region,", 2, 5

"Ending segment for generic BOD initialization for each region,", 4, 7

"Initial concentration for generic BOD per region mg/l,",0.65, 0.75

"Initial concentration for generic BOD per region mg/l,",0.75, 0.85

"Initial concentration for generic BOD per region mg/l,",0.85, 0.65

"Number of regions for different generic sediment BOD constituent consumption rate,", 2

"Starting segment for generic BOD consumption for each region,", 2, 5

"Ending segment for generic BOD consumption for each region,", 4, 7

"Consumption rate for generic BOD per region 1/d,",0.065, 0.065

"Consumption rate for generic BOD per region 1/d,",0.065, 0.065

"Consumption rate for generic BOD per region 1/d,",0.065, 0.065

"Temperature coefficient for generic BOD decay per region,",1.01, 1.01

"Temperature coefficient for generic BOD decay per region,",1.02, 1.02

"Temperature coefficient for generic BOD decay per region,",1.03, 1.03

"Number of regions for different diagenesis related rates,", 2

"Starting segment for regions,", 2, 5

"Ending segment for regions,", 4, 7

"Fraction of labile poc for each diagenesis region,",0.65, 0.65

"Fraction of refractory poc for each diagenesis region,",0.25, 0.25

"Fraction of labile pon for each diagenesis region,",0.65, 0.65

"Fraction of refractory pon for each diagenesis region,",0.2, 0.2

"Pore water diffusion coefficient m²/d,",0.001,0.001

"DO Threshold for aerobic layer oxidation rates mgO2/l,",2.0,2.0

"Nitrification rate in aerobic layer (NH3->NO3) at DO below threshold m/d,",0.131, 0.131

"Nitrification rate in aerobic layer (NH3->NO3) at DO above threshold m/d,",0.131, 0.131

"Denitrification rate in aerobic layer (NO3->N2) at DO below threshold m/d,",0.1 ,0.1

"Denitrification rate in aerobic layer (NO3->N2) at DO above threshold m/d,",0.1 ,0.1

"Denitrification rate in anerobic layer (NO3->N2) m/d,",0.1 ,0.1

"Methane oxidation rate in aerobic layer m/d,",0.7, 0.7

"Nitrification half-saturation constant for NH4N in aerobic layer mgN/l,",0.728,0.728

"Nitrification half-saturation constant for O2 in aerobic layer mgO2/l,",0.37,0.37

"Temperature coefficient for pore water diffusion between layers,",1.08, 1.08

"Temperature coefficient for nitrification,",1.123, 1.123

"Temperature coefficient for denitrification,",1.08, 1.08

"Temperature coefficient for methane oxidation,",1.079, 1.079

"Sulfate concentration above which sulfide over methane is produced mgS/l,",20.0, 2.0

"Sulfide oxidation rate in aerobic layer m/d,",0.2, 0.2

"Temperature coefficient for sulfide oxidation,",1.08, 1.08

"Sulfide oxidation normalization constant for O2 mgO2/l,",4.0, 4.0

"Mineralization rate for labile PON 1/d,",0.035, 0.035

"Mineralization rate for refractory PON 1/d,",0.0018, 0.0018

"Mineralization rate for inert/slow refractory PON 1/d,",0.0, 0.0

"Mineralization rate for labile POC 1/d,",0.035, 0.035

"Mineralization rate for refractory POC 1/d,",0.0018, 0.0018

"Mineralization rate for inert/slow refractory POC 1/d,",0.0, 0.0

"Temperature coefficient for labile PON,",1.1, 1.1

"Temperature coefficient refractory PON,",1.15, 1.15

"Temperature coefficient inert/slow refractory PON,",1.17, 1.17

"Temperature coefficient labile POC,",1.1, 1.1

"Temperature coefficient refractory POC,",1.15, 1.15

"Temperature coefficient for inert/slow refractory POC,",1.17, 1.17

"Methane production calculation method (0: Analytical, 1: Numerical),", 0, 0

"Equilibrium constant for NH4+ <-> NH3 ionization. Provide as pK,", 9.1

"Equilibrium constant for HS- <-> H2S ionization. Provide as pK,", 9.0

"Henry's constant for NH3d <-> NH3g in atm/M,", 0.0179

"Henry's constant for CH4d <-> CH4g in atm/M,", 469

"Henry's constant for H2Sd <-> H2Sg in atm/M,", 10

"Henry's constant for CO2d <-> CO2g in atm/M,", 29

"Gas diffusion coefficient in sediment in m²/s,", 1.0d-9

"Calibration parameter R1 in m,", 0.0014

"Young's modulus E in N/m²,", 1.4d+9

"Critical stress intensity factor for sediments K1c in N/m^3/2,", 300

"Bubbles release scale,", 0.02

"Fraction of critical pressure at which cracks close,", 0.20

"Switch to limit bubble size,", .TRUE.

"Maximum bubble radius in mm,", 80

"Switch to use slow release of bubbles,", .TRUE.

"Bubbles release fraction (sediments),", 0.005

"Bubbles accumulation fraction,", 0.1

"Number of bubbles release array,", 2000

"Bubbles release fraction (atmosphere),", 0.001

"Bubbles-Water gas exchange rate (1/s),",1.0d-7

"Apply additional turbulence due to bubbles release,",.TRUE.

"Turbulence scaling factor for bubbles release,",0.001

"Coefficient Aturb in Aturb*ln(TSS) + Bturb = ln(Turbidity),",1.243

"Coefficient Bturb in Aturb*ln(TSS) + Bturb = ln(Turbidity),",-0.294

"Write sediment fluxes,", .TRUE.

\\cal1-s-filesrv1.golder.gds\data\active_2009\1336\09-1336-1008 - cema pit lake model\reporting\draft 2 may 2011\app b sample input.doc

APPENDIX C

Output File Description

August 2010
Report No. 09-1336-1008

Note: All output files are written at the frequency of the W2 snapshot output and for the specified snapshot intervals specified in the W2 control file.

CEMABottomLayer.opt

This file outputs the model bottom layer for each W2 model segment.

Example

```
    1    2    3    4    5    6    7    8    9   10   11

Bottom Layer (KB)

JDAY =    64.51

   10   10   10   10   10   10   10   10   10   10   10

Bottom Layer (KB)

JDAY =    65.00

   10   10   10   10   10   10   10   10   10   10   10

Bottom Layer (KB)

JDAY =    65.50

   10   10   10   10   10   10   10   10   10   10   10

Bottom Layer (KB)

JDAY =    66.00

   10   10   10   10   10   10   10   10   10   10   10
```

CEMABubbles.opt

This file provides the following output for each W2 model segment:

1. Radius of bubbles
2. Concentration of gasses in the bubble
3. Concentration of dissolved gasses in porewater
4. Net concentration of gas (dissolved + gas) in sediments

Example

CEMA Sediment Bubbles Output

********** JDAY = 64.51

1	2	3	4	5	6	7	8	9	10	11

Radius (mm)

0.00000	0.97979	0.97979	0.97979	0.97979	0.97979	0.97979	0.97979	0.97979	0.97979	0.00000

Cg (gm/m³)

0.0000	0.0000	0.0000	0.0000	0.0000	0.0007	0.0007	0.0007	0.0007	0.0007	0.0000

C0 (gm/m³)

0.0000	0.0001	0.0001	0.0001	0.0001	0.0008	0.0008	0.0008	0.0008	0.0008	0.0000

Ct (gm/m³)

0.0000	0.0001	0.0001	0.0001	0.0001	0.0014	0.0014	0.0014	0.0014	0.0014	0.0000

Crack Open

NO	NO	NO	NO	NO	NO	NO	NO	NO	NO	NO

CEMABubblesAtmosphereRelease.opt

This file provides the gas release rate (gm/s) to the atmosphere due to bursting of gas bubbles at the lake surface for each W2 model segment.

Example

Gas Release to Atmosphere at JDAY = 64.51

1	2	3	4	5	6	7	8	9	10	11
H2S Release(gm/s)										
0.000	0.000	0.000	0.000	0.000	0.000	0.000	0.000	0.000	0.000	0.000
CH4 Release (gm/s)										
0.000	0.000	0.000	0.000	0.000	0.000	0.000	0.000	0.000	0.000	0.000
NH3 Release (gm/s)										
0.000	0.000	0.000	0.000	0.000	0.000	0.000	0.000	0.000	0.000	0.000
CO2 Release (gm/s)										
0.000	0.000	0.000	0.000	0.000	0.000	0.000	0.000	0.000	0.000	0.000

CEMADiagenesisAerobicLayer.opt

This file provides internally calculated thickness for the aerobic layer for each W2 model segment. The oxygen penetration is limited only to the thickness of this layer in the sediments.

Example

```
JDAY =   81.50

     1      2      3      4      5      6      7      8      9     10     11

H1 (m)

  0.00000  0.16701  0.16492  0.16290  0.15969  0.12366  0.12026  0.11766  0.11623  0.11580  0.00000

JDAY =   82.00

     1      2      3      4      5      6      7      8      9     10     11

H1 (m)

  0.00000  0.16688  0.16423  0.15862  0.15409  0.11930  0.11687  0.11509  0.11349  0.11188  0.00000
```

CEMADiagenesisConstituent.opt

This file provides the concentration for organic matter remaining in the MFT bed for each W2 model segment. As noted previously, the organic matter goes through diagenesis and as a result gets depleted from the MFT bed.

Example

JDAY = 64.51

1 2 3 4 5 6 7 8 9 10 11

POC (mg/l)

0.00000 69.99660 69.99660 69.99660 69.99660 79.99612 79.99612 79.99612 79.99612 79.99612 0.00000

JDAY = 64.51

1 2 3 4 5 6 7 8 9 10 11

PON (mg/l)

0.00000 99.99516 99.99516 99.99516 99.99516 79.99613 79.99613 79.99613 79.99613 79.99613 0.00000

JDAY = 64.51

1 2 3 4 5 6 7 8 9 10 11

SO4 (mg/l)

0.00000 1.50000 1.50000 1.50000 1.50000 9.99997 9.99997 9.99997 9.99997 9.99997 0.00000

CEMADiagenesisSOD.opt

This file provides sediment oxygen demand (SOD) exerted by each component of the organic matter for each W2 model segment. Following are the three SOD components written out:

1. CSOD
2. NSOD
3. SOD (CSOD+NSOD)

Example

```
JDAY =   64.51
     1      2      3      4      5      6      7      8      9     10     11
SOD (gO2/m2/d)
 0.00000 0.03240 0.03240 0.03240 0.03240 0.00000 0.00000 0.00000 0.00000 0.00000 0.00000
JDAY =   64.51
     1      2      3      4      5      6      7      8      9     10     11
CSOD (gO2/m2/d)
 0.00000 0.03076 0.03076 0.03076 0.03076 0.00000 0.00000 0.00000 0.00000 0.00000 0.00000
JDAY =   64.51
     1      2      3      4      5      6      7      8      9     10     11
NSOD (gO2/m2/d)
 0.00000 0.00164 0.00164 0.00164 0.00164 0.00000 0.00000 0.00000 0.00000 0.00000 0.00000
```

CEMALogFile.opt

This is a log file that provides information regarding layer addition. The file has times and segment numbers for which model layers were added due to bed consolidation.

Example

```
Layer added at Segment Number      2 on   137.500000000000
Layer added at Segment Number      3 on   137.500000000000
Layer added at Segment Number      4 on   137.500000000000
Layer added at Segment Number      5 on   137.500000000000
Layer added at Segment Number      6 on   137.500000000000
Layer added at Segment Number      7 on   137.500000000000
Layer added at Segment Number      8 on   137.500000000000
Layer added at Segment Number      9 on   137.500000000000
Layer added at Segment Number      10 on   137.500000000000
```

CEMAOutput.opt

This file provides the following output for each W2 model segment:

1. Bed elevation (m): Actual bed elevation
2. Bed elevation layer (m): This is the relative bed elevation from the existing KB
3. Bed porosity (%)
4. Total MFT volume (m^3)
5. Total porewater volume (m^3)
6. Total porewater removed due to consolidation (m^3)

Example

Bed elevation(m)

JDAY = 93.000000

1	2	3	4	5	6	7	8	9	10	11
10.00000	9.21939	9.21938	9.21937	9.21937	9.21936	9.21935	9.21934	9.21933	9.21932	10.00000

Bed elevation layer(m)

JDAY = 93.000000

1	2	3	4	5	6	7	8	9	10	11
0.00000	-0.78061	-0.78062	-0.78063	-0.78063	-0.78064	-0.78065	-0.78066	-0.78067	-0.78068	0.00000

Bed porosity (%)

JDAY = 93.00

1	2	3	4	5	6	7	8	9	10	11
80.00000	78.30596	78.30596	78.30596	78.30596	78.30595	78.30595	78.30595	78.30595	78.30595	80.00000

Total Volume of Sediments = 0.291608E+07 m^3

Total Porewater Volume = 0.105257E+08 m^3

Total Porewater Removed = 0.308250E+02 m^3

CEMASedimentGas.opt

This file provides gas concentration in bubbles for each W2 model segment.

Example

Gas concentration (gm/m³) at JDAY = 65.50

H2S Concentration (gm/m³)

0.000 3.029 3.029 3.029 3.029 3.069 3.069 3.070 3.070 3.072 0.000

CH4 Concentration (gm/m³)

0.000 0.000 0.000 0.000 0.000 0.000 0.000 0.000 0.000 0.000 0.000

NH3 Concentration (gm/m³)

0.000 1.012 1.012 1.012 1.012 0.809 0.809 0.809 0.809 0.810 0.000

CO2 Concentration (gm/m³)

0.000 0.152 0.152 0.152 0.152 0.153 0.153 0.153 0.153 0.153 0.000

CEMAGenBOD.opt

This file provides generic BOD concentrations for aerobic and anaerobic layers for each W2 model segment.

Example

########## JDAY = 65.50 ##########

1 2 3 4 5 6 7 8

Aerobic Layer

SBOD1

0.0000 0.6097 0.6081 0.6082 0.7077 0.7077 0.7077 0.0000

SBOD2

0.0000 0.7081 0.7064 0.7064 0.8073 0.8074 0.8074 0.0000

SBOD3

0.0000 0.8072 0.8052 0.8053 0.6210 0.6210 0.6210 0.0000

Anaerobic Layer

SBOD1

0.0000 0.6491 0.6491 0.6491 0.7495 0.7495 0.7495 0.0000

SBOD2

0.0000 0.7490 0.7490 0.7490 0.8494 0.8494 0.8494 0.0000

SBOD3

0.0000 0.8489 0.8489 0.8489 0.6496 0.6496 0.6496 0.0000

\\cal1-s-filesrv1.golder.gds\data\active_2009\1336\09-1336-1008 - cema pit lake model\reporting\draft 2 may 2011\app c output files.doc

At Golder Associates we strive to be the most respected global group of companies specializing in ground engineering and environmental services. Employee owned since our formation in 1960, we have created a unique culture with pride in ownership, resulting in long-term organizational stability. Golder professionals take the time to build an understanding of client needs and of the specific environments in which they operate. We continue to expand our technical capabilities and have experienced steady growth with employees now operating from offices located throughout Africa, Asia, Australasia, Europe, North America and South America.

Africa	+ 27 11 254 4800
Asia	+ 852 2562 3658
Australasia	+ 61 3 8862 3500
Europe	+ 356 21 42 30 20
North America	+ 1 800 275 3281
South America	+ 55 21 3095 9500

solutions@golder.com
www.golder.com

Golder Associates Ltd.
102, 2535 - 3rd Avenue S.E.
Calgary, Alberta, T2A 7W5
Canada
T: +1 (403) 299 5600

Golder Associates